REVIEW ARTICLE

Three-dimensional electron microscopy techniques for unravelling mitochondrial dysfunction in heart failure and identification of new pharmacological targets

Correspondence Dr Ashraf Kitmitto, Division of Cardiovascular Sciences, Faculty of Biology, Medicine and Health, University of Manchester, AV Hill, Dover Street, Manchester M13 9PL, UK. E-mail: ashraf.kitmitto@manchester.ac.uk

Hussam M Daghistani [iD], Bodour S Rajab [iD] and Ashraf Kitmitto [iD]

Division of Cardiovascular Sciences, School of Medical Sciences, Faculty of Biology, Medicine and Health, The University of Manchester, Manchester Academic Health Science Centre, Manchester, UK

A hallmark of heart failure is mitochondrial dysfunction leading to a bioenergetics imbalance in the myocardium. Consequently, there is much interest in targeting mitochondrial abnormalities to attenuate the pathogenesis of heart failure. This review discusses (i) how electron microscopy (EM) techniques have been fundamental for the current understanding of mitochondrial structure–function, (ii) the paradigm shift in resolutions now achievable by 3-D EM techniques due to the introduction of direct detection devices and phase plate technology, and (iii) the application of EM for unravelling mitochondrial pathological re-modelling in heart failure. We further consider the tremendous potential of multi-scale EM techniques for the development of therapeutics, structure-based ligand design and for delineating how a drug elicits nanostructural effects at the molecular, organelle and cellular levels. In conclusion, 3-D EM techniques have entered a new era of structural biology and are poised to play a pivotal role in discovering new therapies targeting mitochondria for treating heart failure.

LINKED ARTICLES

This article is part of a themed section on Mitochondrial Pharmacology: Featured Mechanisms and Approaches for Therapy Translation. To view the other articles in this section visit http://onlinelibrary.wiley.com/doi/10.1111/bph.v176.22/issuetoc

Abbreviations

2-D, two-dimensional; 3-D, three-dimensional; Cryo-ET, cryo-electron tomography; DED, direct electron detection; Drp1, dynamin-related protein 1; EM, electron microscopy; ET, electron tomography; ETC, electron transport chain; FEG, field emission gun; FIB-SEM, focussed ion beam scanning; Higd-1a, hypoxia-induced gene domain protein-1a; IBM, inner boundary membrane; IFM, interfibrillar mitochondria; IMJ, inter-mitochondrial junction; IMM, inner mitochondrial membrane; IMS, intermembrane space; Mfn1, mitofusin 1; Mfn2, mitofusin 2; MICOS, mitochondrial contact site and cristae organizing system; mNT, mitoNEET; mtDNA, mitochondrial genome; OMM, outer mitochondrial membrane; Opa1, optic atrophy gene; OXPHOS, oxidative phosphorylation; PNM, perinuclear mitochondria; SBF-SEM, serial block face scanning; SEM, scanning electron microscopy; SPA, single particle analysis; SR, sarcoplasmic reticulum; SSM, subsarcolemmal mitochondria; TEM, transmission electron microscopy

Introduction

It is estimated that over 26 million people worldwide suffer from heart failure, a major cause of mortality and morbidity (Ponikowski *et al.,* 2014). Heart failure is a chronic condition, whereby the heart is damaged so that it is unable to effectively pump blood to meet systemic metabolic demands (Minicucci *et al.,* 2011). Moreover, ageing is now known to be closely associated with heart failure with an estimated 10-fold increase in risk over the age of 60 (Strait and Lakatta, 2012). Since the proportion of the population classified as elderly (60+ years) is the fastest growing age group across the world (World Health Organization, www.who.int), the number of heart failure patients is set to rise at an alarming rate; in Western countries, it is estimated that by 2050, approximately a quarter of the population will be older than 60, and in some places the elderly may account for nearly 50% (www.globalaging.org/waa2). Heart failure also impacts upon overall patient health leading to the development of other co-morbidities including atrial fibrillation, ventricular tachycardia (associated with sudden cardiac death) (Luu *et al.,* 1989; Ayesta *et al.,* 2018), cardiac cachexia (Okoshi *et al.,* 2017) and with congestion contributing to renal failure (Afsar *et al.,* 2016). Moreover, patients with diabetes also have an increased risk of developing heart failure, with a 10-fold increase in mortality rates and with a drop in 5-year survival from 50% in non-diabetic patients (Cleland *et al.,* 2005) to only 12.5% (Khan *et al.,* 2014). Significantly, the number of cases of type 2 diabetes is rising at an alarming rate, with data from the World Health Organization reporting that the number of diabetics has quadrupled from 1980 to 422 million in 2014. The projections for an increasing prevalence of type 2 diabetes in the coming years will thus add considerably to the heart failure burden.

Although there are different types of heart failure, also termed congestive heart failure, which present as either preserved or reduced ejection fraction, the main pharmacological treatments, β-blockers, **ACE** inhibitors, **angiotensin receptor** blockers (ARBs), **aldosterone** antagonists, **digoxin** and diuretics remain the mainstay for disease management. These drugs work mainly to alleviate the cardiac load to address the imbalance between energy supply and demand, providing symptomatic relief and delay in disease progression but with little impact upon mortality rates. Notably, a recent study revealed that there has been no improvement in heart failure survival rates over the last 20 years (Taylor *et al.,* 2017). Recently, there has been some new heart failure treatments introduced with, for example, the approval of Entresto in 2015 by the European Medicines Agency and FDA for the treatment of chronic heart failure with reduced ejection fraction. Entresto is a dual action drug, combining **valsartan** with **sacubitril** to target the renin-angiotensin-aldosterone system and inhibit **neprilysin** respectively (Fala, 2015). **Corlanor** (ivabradine) was also approved for usage in 2015 for treating symptomatic chronic heart failure (with an ejection fraction of ≤35%) usually in combination with β-blockers. Corlanor reduces the heart rate by blocking the 'pacemaker channel' **HCN4** (Oliphant *et al.,* 2016). However, none of these drugs specifically target the progressive structural remodelling events shown to be a characteristic feature of heart failure (Gonzalez *et al.,* 2011). A hallmark of heart failure is a progressive decline in left ventricular contractility due in part to the adverse changes to cellular ultrastructure; however, a major hindrance for the development of new heart failure treatments is that the mechanisms underpinning disease progression at the nanostructural level still remain largely unknown.

Mitochondrial dysfunction is linked to heart failure development

In order for the heart to beat, cardiomyocytes require a continuous supply of energy in the form of **ATP**, which is provided by the mitochondria (Dorn, 2013a). Consequently, due to the high energy demands of the heart, cardiomyocytes have a higher number of mitochondria than any other cell type, with mitochondria occupying around a third of the cardiomyocyte volume (Bugger and Abel, 2010). Failure of mitochondria to produce sufficient ATP is linked to cardiac cell death and myocardial infarction, a leading cause of heart failure (Kubli and Gustafsson, 2012). Thus, preserving mitochondrial function is integral to protecting cardiac function. Significantly, mitochondrial dysfunction starts to occur in hypertrophy and in the early stages of heart failure making it an attractive therapeutic target for attenuating heart failure progression (Facundo *et al.,* 2017). Changes to substrate utilization, ion homeostasis and an elevated production of ROS are all mitochondrial abnormalities of heart failure that have been discussed at length elsewhere (and recently reviewed by Brown *et al*., 2017). Therefore, this article, in keeping with the structural theme, will focus upon the molecular and cellular remodelling events that lead to changes to the mitochondrial membrane infrastructure and consequently the spatial distribution and diffusion of proteins and cofactors that collectively underpin the development of impaired oxidative phosphorylation (OXPHOS) and ATP production.

In Table 1, we have listed some exemplar studies reporting changes to the size and structure of mitochondria, identifying small fragmented mitochondria and abnormal cristae structure, illustrating that they are common features of both clinical and animal models of heart failure and diabetes. It is noteworthy that most of the studies in Table 1 pertain to animal or cell-based models of heart failure, or cardiovascular pathologies that ultimately lead to heart failure, such as myocardial infarction and diabetes, highlighting a further complication of studying the pathogenesis of heart failure and development of new treatments, namely, the lack of access to human samples. Human cardiac tissue can be obtained during certain procedures, such as implantation of left ventricular assist devices, or from donated non-transplantable human hearts and explanted failing hearts, but these are limited in availability. Additional factors such as small sample sizes, differences in patient age, sex and predisposing factors, for example, associated diseases, genetics and medication regimens, have led to the development and wide use of small and large animal models in experimental studies. Although no animal model will completely replicate all features of the human condition, animal models still represent powerful tools for the study of a wide spectrum of cardiovascular

Table 1

Examples of studies reporting changes to mitochondrial morphology in human heart failure and diabetes, animal models of disease and following genetic ablation, and *in vitro* models of ischaemia

Species	Pathology	Mitochondrial morphology	Reference
Human and rat	Heart failure	Small and fragmented	Chen *et al.* (2009)
Human endomyocardial biopsy	Congestive heart failure	Increase in mitochondrial number and variation in size. Partial degeneration of the cristae	Takemura *et al.* (2016)
Human biopsy	Dilated cardiomyopathy	Abnormal circular cristae	Mudhar *et al.* (2001)
Canine	Heart failure	Decreased amount of the major mitochondrial (respirasome I/III$_2$/IV). The amounts of free Complexes I and III were increased in SSM	Rosca *et al.* (2008)
New Zealand female rabbits	Ischaemic heart disease	Swollen mitochondria with disorganized cristae	Abbate *et al.* (2007)
Rat	Acute myocardial infarction	Swollen mitochondria. Loss of cristae	Hollander *et al.* (2016)
Rat	Ischaemic reperfusion injury	Moderately swollen mitochondria	Cao *et al.* (2016)
db/*db* mouse	Type 2 diabetes	Increase in mitochondrial number and smaller sizes	Boudina *et al.* (2007)
24-week-old Akita mouse	Type 1 diabetes	Reduced cristae density, increased mitochondrial volume; mitochondrial number unchanged	Bugger *et al.* (2008)
12-week-old Akita mouse	Type 1 diabetes	Reduced cristae density, increase in mitochondrial volume and number	Bugger *et al.* (2009)
OVE26 mouse	Type 1 diabetes	Severely damaged mitochondria	Ye *et al.* (2004)
OVE26 mouse	Type 1 diabetes	Increased mitochondrial area and number with severe damage to mitochondria	Shen *et al.* (2004)
UCP-DTA mouse	Metabolic syndrome	Increase in mitochondrial size and increased mitochondrial volume and density	Duncan *et al.* (2007)
CIRKO mouse	Transgenic diabetes	Dysmorphic with reduced cristae density. Increased mitochondrial number/density and volume	Boudina *et al.* (2009)
Human biopsy	Diabetic cardiomyopathy	Aggregated mitochondria	Saito *et al.* (2015)
Mouse	PINK1-defecient KO	Mitochondrial swelling	Kubli *et al.* (2013)
Mouse	Mfn1 and Mfn2 ablations	Fragmented mitochondria	Chen *et al.* (2011b)
Cell type	**Model**	**Mitochondrial morphology**	**Reference**
H9c2 cardiac myogenic cell line	Ischaemia	Fragmented mitochondria	Chen *et al.* (2009)
Cardiac HL-1 cells	Ischaemia	Fragmented mitochondria	Ong *et al.* (2010)
H9c2 cells	Exposure to nucleoside reverse transcriptase inhibitors (NRTI) (anti-retroviral)	Mitochondrial swelling and disorganization. Loss of cristae	Liu *et al.* (2012)

diseases, with the ability to also generate transgenic models to investigate molecular alterations, and as such play a pivotal role in preclinical research. For detailed evaluations of the application of large and small animals for the study of cardiovascular disease, see reviews by Camacho *et al.* (2016) and Milani-Nejad and Janssen (2014).

Unlike non-muscle cells, cardiac mitochondria can be regarded as spatially distinct populations: interfibrillar mitochondria (IFM), those mitochondria embedded between myofibrils; subsarcolemmal mitochondria (SSM), mitochondria situated underneath the cell membrane (sarcolemma); and perinuclear mitochondria (PNM), mitochondria around the nucleus (Hollander *et al.,* 2014). Although the concept of spatially separated mitochondria has recently been challenged by a study from Rassaf and colleagues who, using two-dimensional (2-D) images from standard transmission electron microscopy (TEM) of thin sections prepared from rat left ventricle, showed that all mitochondria are interconnected and thus they are not separate populations (Hendgen-Cotta *et al.,* 2018). Our study of an ovine tachypacing-induced model of end-stage heart failure indicated that the IFM were rearranged to form large clusters (Pinali *et al.,* 2013). How these populations are affected as heart failure progresses is not currently fully understood.

TEM has played a central role for characterizing mitochondrial morphology and function

It was approximately 75 years ago that some of the first images of isolated mitochondria from rat neoplastic cells were captured using TEM, revealing a spherical morphology with diameters ranging from 0.5 to 1.5 μm (Claude and Fullam,

1945). In a transmission electron microscope, the electrons are focussed into a beam, which contacts with the specimen, some of the electrons are scattered, and the 'transmitted' unscattered electrons that pass through the specimen are detected and a 2-D image is formed (generally referred to as standard, conventional, TEM). Standard TEM methods have revealed that the shape and size of mitochondria are highly variable between prokaryotic and eukaryotic cells. In mammals, mitochondrial size is tissue-dependent, for example, liver mitochondria range from 0.5 to 5 μm in length whereas cardiac mitochondria are typically restricted in length by the dimensions of the sarcomere, that is, 1.5–2 μm (Perkins and Frey, 2000; McCarron *et al.,* 2013). Seminal TEM studies in the 1950s further revealed that mitochondria have an inner membrane that is folded to form 'baffle' like invaginations extending inward which were named *cristae mitochondriales* (Palade, 1952; Sjostrand, 1956). Since then, TEM has been instrumental for establishing that mitochondria are composed of an outer mitochondrial membrane (OMM) and inner mitochondrial membrane (IMM) separated by the intermembrane space (IMS), with the IMM forming the cristae and with the volume encompassed by the IMM called the matrix. The folding of the IMM to form cristae provides a large surface area, a structural property fundamental for propagating signalling pathways underpinning the bioenergetic properties of mitochondria.

It is now clear that the unique structure of mitochondria with separate compartments is central for controlling a wide range of cellular processes, such as, β-oxidation, glycolysis, citric acid cycle and the generation of ATP by OXPHOS. For example, central to energy provision in the heart is the β-oxidation of long-chain fatty acids, with a series of enzymatic steps starting with uptake of plasma fatty acids and carnitine into the cardiomyocyte cytosol, leading to the formation of acyl-CoA esters, which are transported across the OMM into the IMS followed by translocation of fatty acyl moieties, with the end products entering the citric acid cycle. Similarly, while glycolysis occurs in the cytosol postglycolytic reactions within the mitochondria fuel the citric acid cycle, with enzymes forming the citric acid cycle located within the matrix, with the production of **NADH** and $FADH_2$ essential substrates for OXPHOS. OXPHOS is regulated by the electron transport chain (ETC), membrane protein complexes located within the IMM. The IMM barrier also facilitates the formation of the proton gradient that drives OXPHOS. The ETC consists of Complex I, II, III, IV, V, ubiquinone Q and **cytochrome C** and co-factors. Crucially, it is the spatial organization of the ETC components within the cristae, which underpins the sequential redox reactions forming the proton gradient that drives ATP production (Chaban *et al.,* 2014).

Significantly, TEM studies have revealed that cristae morphology varies between cardiac mitochondrial populations; SSM are reported to have a lamelliform cristae (Shimada *et al.,* 1984; Riva *et al.,* 2005; Hollander *et al.,* 2014), whereas IFM and PNM are thought to mostly have tubular cristae (Riva *et al.,* 2005). Moreover, several groups have proposed that there are functional differences between each population; for example, IFM are shown to have higher respiration rates and ATP production, which may be an adaptation/optimization for facilitating muscle contraction

(Schwarzer *et al.,* 2013; Hatano *et al.,* 2015). Crochemore *et al.* (2015) also reported that levels of ROS are higher in SSM.

It is now well-established that changes to the size, shape and organization of mitochondria occur in response to a number of cardiac pathologies, with TEM methods instrumental for advancing current understanding of mitochondrial remodelling. However, there remains a lack of clarity surrounding the mechanisms that promote mitochondrial dysfunction in heart failure. Moreover, to develop new pharmacological agents targeting specific mitochondrial proteins knowledge of the three-dimensional (3-D) protein structure is essential for the design of compounds with high specificity and activity, limiting off-target effects, as is the structural infrastructure in which the protein functions to direct cellular processes. Advances in high throughput technologies and the advent of the genomics and proteomics era coupled with big data handling have revitalized the structure-based drug race. However, a key rate-limiting step has been the transfer of linear genetic and protein information into a 3-D functional context. The following sections will consider how multi-scale 3-D EM methods (from molecules to organelles to cells) have contributed towards the existing body of knowledge on mitochondrial function and dysfunction, the impact of the recent technological advances and the potential of these techniques for aiding drug discovery. This review will focus upon three types of 3-D EM techniques that straddle the structural and resolution hierarchy, namely, cryo-EM and single particle analysis (SPA) for the study of isolated proteins and macromolecular complexes, cryo-electron tomography (cryo-ET) for the study of organelle morphology and macromolecular structures *in situ* and two modalities of scanning EM (SEM): serial block face SEM (SBF-SEM) and focussed ion beam SEM (FIB-SEM).

Cryo-EM and SPA techniques enter a new era for protein structural analysis at near atomic resolutions

The ETC Complexes underpinning OXPHOS are macromolecular units each composed of multiple membrane proteins and consequently represent a major challenge for structural study using classical biophysical techniques such as solution NMR and X-ray crystallography. Integral membrane proteins are often recalcitrant to structural investigations due to a number of reasons, including (i) a low abundance in native tissue making purification difficult, (ii) issues of solubility and low yields associated with expression in recombinant systems, (iii) they often contain large extracellular highly flexible domains that are not amenable to forming crystal contacts necessary for X-ray crystallography, and (iv) by forming large macromolecular complexes that are too large to study by standard solution NMR methods. The advantage of studying proteins by TEM is that only micrograms of protein are needed compared to the milligrams typically required for X-ray crystallography and NMR. Furthermore, the protein is imaged in solution, so buffers can be used to stabilize the protein structure or capture a specific conformation, thereby also removing the rate-limit step of crystallization.

However, as electron microscopes operate using high vacuums, biological samples need to be preserved, which led to the development of freezing techniques (Dubochet *et al.,* 1988). In brief, the method involves rapid freezing of the biological sample in an aqueous environment by plunging it into a bath of liquid ethane. The plunge-freezing velocity prevents evaporation of the surrounding water molecules and so stops the water molecules from crystallizing. Therefore, the specimen is imaged in a frozen-hydrated state close to native conditions. However, because proteins are made up of mainly C, H, O and N, atoms that are weakly scattered by the electron beam, they are barely distinguishable from the surrounding water molecules leading to a very low signal: noise in the image. Furthermore, due to biological samples being sensitive to radiation damage, low dose conditions, for example, $<20e^-/Å^2$ at the specimen level, are typically employed, which also leads to reduced contrast. These factors have led to the development of single particle analysis (SPA) methods. The concept of SPA is built upon the premise that in solution, the protein sample adopts random orientations (although occasionally a preferred orientation occurs thought to be due to the sample interacting with the air/water interface). In brief, tens of thousands of particles, that is, copies of the same object (the protein) presenting different angular views are selected, which are then sorted into groups according to their orientation (a class), with the particles in each group averaged to form a single image (termed a class average). The class average will therefore have a much higher signal: noise. As the class averages show different orientations of the protein, they can then be used to generate a 3-D structure. A detailed overview of the theory and technical details of SPA and cryo-EM are outside the scope of this review and can be found elsewhere (e.g. Cheng *et al.,* 2015; Thompson *et al.,* 2016)

Despite the development of computational methods for SPA analysis and the replacement of tungsten filaments with field emission guns (FEG), which produce a more coherent and brighter electron beam, the high noise component within the images still, until recently, limited the structural data to typically between 10 and 15 Å leading cryo-EM to be synonymous with the term 'blobbology'. The introduction of charge-coupled detector cameras greatly enhanced the efficiency of data collection but had the drawback that high-frequency data were degraded through the detection process, thereby also limiting attainable resolutions. However, in the last few years, there has been a 'resolution-revolution' (Kuhlbrandt, 2014) with the advent and application of direct electron detection (DED) devices, to directly detect the electrons so that the high-frequency information in the image is preserved. A further advantage of these devices is the individual frame rate, whereby within a single exposure multiple frames (e.g. 40–50) are collected. From this stack of frames, it is possible to differentiate between single electron events so that noise from beam-induced sample motion (i.e. upon exposure of the sample to the electron beam), or stage drift, can be identified and the relevant frames can be discarded; the remaining frames are then combined to form a single image with a higher signal: noise (McMullan *et al.,* 2016). Subsequently, a number of specialist programmes such as RELION (Fernandez-Leiro and Scheres, 2017) and MotionCor2 (Zheng *et al.,* 2017) have been developed to allow for motion-correction.

In addition to DEDs, a further technological advancement has been the development of the Volta phase plate as reviewed by Danev and Baumeister (2016). Phase plate technology improves low spatial frequencies leading to improved contrast, with the added advantage that lower dose electrons can be used, thereby also minimizing sample damage. A recent study has shown that by collecting phase plate data, the generation of 3-D structures of relatively small proteins (i.e. <100 kDa) at near atomic resolutions are now possible (e.g. Khoshouei *et al.,* 2017b). As a consequence of these developments, there has been an exponential rise in publications of proteins and complex structures solved at near-atomic resolution by cryo-EM and SPA; for a more detailed overview and in-depth discussion of the technical advancements and applications of cryo-EM methods see the recent review by Henderson (2015). In summary, the recent hardware developments coupled with associated computer algorithms and GPU computers have led to a paradigm shift in the application of cryo-EM methods for protein structural analyses, which have opened up new avenues for advancing structure-based drug design. With the recognition of the quantum leap that has been made to this field, the Nobel Prize in Chemistry 2017 was awarded to the three innovators of the methods that underpinned the development of cryo-EM/SPA techniques.

SPA cryo-TEM for analysis of ETC complexes

Using cryo-EM and SPA methods, several high-resolution structures of mitochondrial proteins have now been solved. The structure of Complex I (the largest of the respiratory Complexes, at 970 kDa) isolated from bovine heart mitochondria was recently reported at an overall resolution of 4.2 Å (Zhu *et al.,* 2016) assigning 93% of the 8515 amino acid residues. The same study identified three distinct conformations of Complex I, which provided new insights into the dynamics and mechanisms of enzymatic activity. The same year a cryo-EM 3-D structure for ovine heart Complex I was published at a similar resolution (3.9 Å) also identifying the putative sites of cardiolipin binding. Cardiolipin accounts for up to 18% of the lipid composition of the IMM and is shown to be essential for Complex activity (Sharpley *et al.,* 2006). For many years, it was assumed that each of the ETC complexes existed as individual entities until Schagger and Pfeiffer (2000) showed by blue native-PAGE that the complexes formed higher order assemblies. Consequently, it is now generally accepted that the respiratory Complexes exist as a mixture of free holoenzymes and as supermolecular complexes within the cristae (Acin-Perez *et al.,* 2008) and that there is a critical amount of each complex that is required for the formation of a supercomplex (D'Aurelio *et al.,* 2006). The supercomplex, termed the respirasome, is formed by the proton pumping units, Complex I, a dimer of Complex III and Complex IV ($C1_1CIII_2CIV_1$). Recently, three high-resolution cryo-EM structures (ranging from ~9 to 6 Å resolution) were reported for the respirasome isolated from bovine (Sousa *et al.,* 2016), ovine (Letts *et al.,* 2016) and porcine (Gu *et al.,* 2016) heart. The cryo-EM structures identified all known 80 subunits forming the respirasome and identified the interaction sites between each Complex. These structures revealed the biological significance of supercomplex formation, namely, stabilization of Complex I activity, the efficiency of

electron flow and for ROS production (Maranzana *et al.,* 2013) and thus optimization of OXPHOS. A further development in delineating the spatial organization of the respiratory complexes has been the isolation of a human 'megacomplex' $C_1 2CIII_2CIV_2$ (purified from HEK293F cells) with a 3-D cryo-EM structure determined at close to near atomic resolution (Guo *et al.,* 2017). Additionally, the group identified a volume within the EM envelope that could accommodate Complex II and thus suggested that 'megacomplexes' also incorporating CII can assemble to optimize the transfer of electrons from succinate to NADH.

Impaired activity of several of the ETC complexes has been reported as a feature of heart failure; in explanted hearts from terminal heart failure patients, there was both a reduction in Complex I activity and maximal respiratory capacity compared to non-failing donor hearts, but with no change in the activity of the other Complexes or damage to mitochondrial DNA (Scheubel *et al.,* 2002). More recently, studies employing a canine coronary microembolization-induced heart failure model (Rosca *et al.,* 2008) demonstrated that rather than deficits in activity occurring to individual Complexes, a reduction in OXPHOS was due to an impairment of respirasome macromolecular assembly and content. A loss of integrity and stoichiometry of respiratory supercomplex organization for optimization of OXPHOS has also been suggested to underpin a decline of cardiac mitochondrial bioenergetics associated with ageing (Gomez *et al.,* 2009).

Many therapeutic approaches have focused upon targeting of increased levels of ROS, formed as a result of deranged ETC and collapse of the mitochondrial membrane potential. Indeed, there are a large number of articles that discuss the strategies for scavenging of ROS, the disappointing clinical trials of systemic antioxidants and the potential of compounds that specifically target mitochondrial ROS production as an approach for treating heart failure, as discussed by Dietl and Maack (2017). The high-resolution 3-D structures of the respirasome recently generated by cryo-EM methods have revealed atomic resolution data previously not available and consequently will be pivotal for contributing to the ongoing quest towards understanding the mechanisms of electron transport and substrate channelling. The structures now provide details of the amino acids that form the interfaces between the various subunits within a Complex as well as the interacting regions between each Complex. These data will now greatly aid efforts for developing new approaches to stabilizing supercomplex assembly as well as biogenesis through targeting specific amino acids and domains. The structures will also provide new insights as to the impact of post-translational modifications and, for example, single point mutations and effects on gain or loss of function. Studies have indicated that respiratory supercomplex formation occurs in stages (Moreno-Lastres *et al.,* 2012) and, consequently, the factors that stabilize higher order assemblies are currently an intensely pursued area of research (Winge, 2012; Lobo-Jarne and Ugalde, 2018). Since a breakdown in supercomplex assembly and formation of different stoichiometries have been shown to be a feature of heart failure and the ageing heart, then targeting the mechanisms of higher order Complex assembly has potential as a new

important therapeutic approach to maintain OXPHOS efficiency and minimize excessive ROS generation.

SPA cryo-EM for analysis of protein regulators of mitochondrial dynamics

Until fairly recently, it was thought that cardiac mitochondria were static due to the dense myofilament arrangement, but there is now a large body of evidence to indicate that mitochondria undergo fission, fusion, motility, biogenesis and mitophagy; processes crucial for regulating mitochondrial size, shape, organization, the maintenance of the mitochondrial genome (mtDNA) and the expulsion of damaged mitochondria *via* mitophagy (Dorn, 2013b). Fusion of the outer membrane between two mitochondria is regulated by mitofusin 1 (Mfn1), mitofusin 2 (Mfn2), followed by fusion of the inner membrane mediated by optic atrophy gene, Opa1, as illustrated in Figure 1A. Fission is under the control of dynamin-related protein 1 (Drp1) (Chen *et al.,* 2011). The fusion and fission proteins are all GTPases. Mfn2 also has, yet to be fully understood, pleiotropic roles in mitophagy, as a protein bridge linking mitochondria to the sarco/endoplasmic reticulum and in apoptosis (Dorn, 2013b). Fusion leads to the amalgamation of two adjacent mitochondria facilitating the exchange of content as part of a quality control process to maintain optimally functional mitochondria, whereas fission leads to smaller mitochondria and isolates damaged organelles for mitophagy or apoptosis (Rimbaud *et al.,* 2009). The balance between fission and fusion regulate the morphology of mitochondria. Defective mitochondrial dynamics has also been identified as a feature of heart failure (Knowlton and Liu, 2015) and diabetic cardiomyopathy (Galloway and Yoon, 2015). Hausenloy and colleagues have further reported that the promotion of fusion (and inhibition of fission) is cardioprotetive against ischaemia reperfusion injury (Ong *et al.,* 2010).

Small fragmented mitochondria that are dysfunctional and generators of ROS have been observed in a range of cardiac pathologies (Table 1) as well as, for example, a feature of neurodegenerative diseases (Cherubini and Gines, 2017). Pertinently, heart failure and neurodegenerative diseases often are coincident with studies indicating that heart failure is associated with an increased risk of dementia (Wolters *et al.,* 2018). Therefore, a better understanding of common inter-linked pathologies may offer new diagnostic and treatment opportunities. Consequently, there has been significant interest in the development of Drp1 inhibitors, since the binding of Drp1 to receptors on the OMM is a key event that triggers the division of one mitochondrion into two smaller mitochondria. The most studied inhibitor is probably Mdivi-1, a quinazolinone, discovered by Cassidy-Stone *et al.* (2008) and shown to be selective for inhibition of Drp1 activity with a K_i of 1–50 μM. Mdivi-1 has been shown not to directly inhibit GTPase activity and is suggested to instead act allosterically to prevent ring structures forming, which requires GTPase activity. Rather than a structure-based approach to drug design, Cassidy-Stone and colleagues identified Mdivi-1 through dual testing of a small molecule library on yeast growth and effects upon mitochondrial morphology. The specificity of Mdivi-1 has recently been challenged by Bordt *et al.* (2017) who reported that Mdivi-1
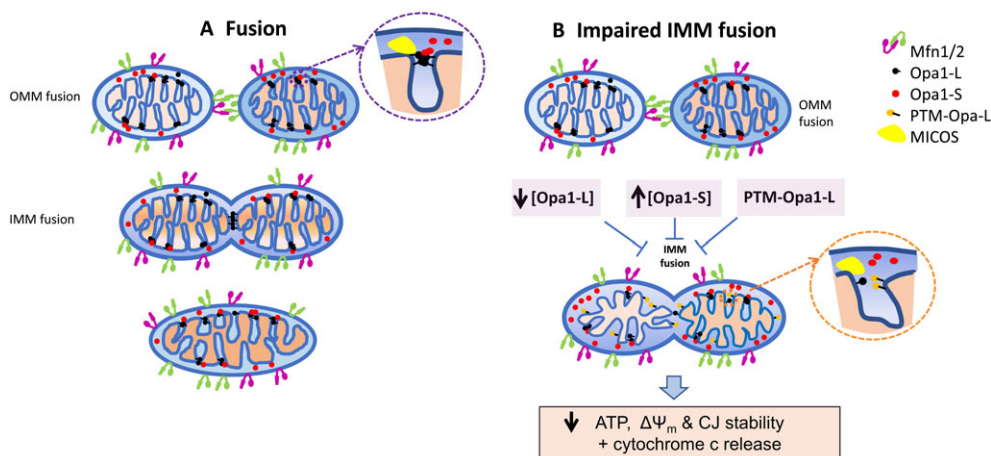
Figure 1

Mitochondrial fusion and the role of Opa1. (A) Fusion between two neighbouring mitochondria is held to be a two-stage process; the first step involves the fusion of the OMM *via* the formation of homodimeric and heterodimeric Mfn2/Mfn2 and Mfn1/Mfn2 complexes. The second step involves the formation of Opa1-L oligomers to drive the fusion of the IMM. *Inset* (red dashed circle) illustrates how oligomers of both the short and long form of Opa1 and association with MICOS form a macromolecular complex important for stabilization of the cristae junctions (CJ). (B) Illustrates how under pathological conditions, based upon multiple studies of cardiovascular disorders linked to heart failure, there is either reduced expression of Opa1-L or proteolytic cleavage of Opa1-L to form Opa1-S and in conditions mimicking diabetic cardiomyopathy post-translational modification (PTM) of Opa-L occurs. Each of these events is reported to result in impaired fusion of the IMM and loss of CJ stability, factors contributing towards mitochondrial dysfunction.

is a reversible inhibitor of Complex I and also leads to ROS production. However, a recent commentary from Smith and Gallo (2017) contends that Mdivi-1 bioactivity may still hold significant promise as a therapeutic agent for manipulating fission, but that further biochemical studies are required to validate the efficacy and specificity in different disease systems and stage of disease progression. The application of Mdivi-1 for treating heart disease has been explored by several groups (Ong *et al.,* 2010; Givvimani *et al.,* 2012; Sharp *et al.,* 2015). One study showed that Mdivi-1 decreased the severity of left ventricular dysfunction in heart failure (Givvimani *et al.,* 2012). Additionally, treatment with Mdivi-1 has also been demonstrated to improve right ventricular function and decrease hypertrophy in hyperproliferative disorders such as pulmonary arterial hypertension by Marsboom *et al.* (2012).

Since the Cassidy-Stone study, a 2.4 Å X-ray crystallographic structure of human dynamin-1 dimer, a homologue of Drp1, has been determined (Frohlich *et al.,* 2013), although the construct lacked the variable domain proposed to mediate binding to the OMM. Through the recent application of cryo-EM and SPA methods by Basu *et al.* (2017), we now have a better understanding of how Drp1 monomers assemble into ring-like structures (predominantly 16-mers) with ring diameters ranging from 20 to 30 nm. While the 3-D EM map of the Drp1 ring is at medium resolution, the structure nevertheless reveals several new key events that regulate fission demonstrating that ring formation is dependent upon GTPase activity but, significantly, that the ring diameter is not sufficiently large enough to encompass the mitochondrial double membrane membranes, each estimated to ~7 nm thick (Perkins *et al.,* 1997), indicating that the mechanism regulating fission may be more complex and involve multiple pathways.

Another approach to prevent Drp1 oligomerization and consequently fission are strategies to prevent Drp1 binding to receptors within the OMM, with Fis-1, MiD49/51 and Mff identified as Drp1 binding partners (Otera *et al.,* 2010; Osellame *et al.,* 2016). Employing this approach, Qi *et al.* (2013) designed a peptide inhibitor, P110, to block the binding of Drp1 to Fis1. The peptide was designed based upon the surface accessibility of protein domains (potential interaction sites) through applying bioinformatic analyses and using the crystal structures of rat dynamin-1 (3ZVR.pdb) and Fis-1 (1NZN.pdb). Using a cell-based and *in vivo* model of Parkinson's disease, P110 was shown to preserve neuronal integrity and viability, and reduce mitochondrial fragmentation (Qi *et al.,* 2013; Filichia *et al.,* 2016). Significantly, P110 has been shown to prevent cardiac dysfunction and protect the heart in a rat model of ischaemic-reperfusion injury (Disatnik *et al.,* 2013). A recent cryo-EM/SPA study has now made a key contribution to this area of research by the generation of a high-resolution (4.2 Å) structure of full-length Drp1 in complex with MiD49 (Kalia *et al.,* 2018). By capturing different conformations of Drp1 associated with GTPase activity, the study provides several new insights into the mechanisms of fission, namely, nucleotide binding to Drp1 is shown to open up and elongate the structure so that receptor binding sites become exposed, binding of Drp1 to MiD49 initiates linear polymerization, and upon GTP hydrolysis, the Drp1 linear filaments are released into the cytosol where they form rings. Structures for each of these conformations were reported, identifying the surfaces and amino acids that regulate the formation of 'constrictor' rings with single point mutations introduced to validate the mechanisms. While it is still not clear how a circular ring of Drp1 oligomers with diameters ~16 nm can cause scission of the OMM and IMM, based

upon the current structures Kalia *et al*. (2018) suggested that constriction of the two membrane leaflets may be a precursor to fission mediated by Drp1 or that fission occurs in stages, with IMM fission occurring prior to OMM fission and/or that Drp1 ring structures may function to optimize membrane curvature to mediate the final steps of fission involving other dynamin-related mechanisms. The generation of high-resolution Drp1 structures in different nucleotide bound states has allowed identification of the oligomerization domains at near atomic resolution as well as at the receptor binding interface. These data will be extremely valuable for the design of new compounds to block Drp1 ring formation, potentially through binding to the oligomerization interface and also allow further investigations of how existing drugs such as Mdivi-1 that inhibit fission may be optimized with reduced off-target effects.

The activity of Drp1 has also been associated with post-translational modifications (Archer, 2013). An increase in Drp1 activity, which leads to fission, has been linked to the phosphorylation of serine 616 (Taguchi *et al.*, 2007; Marsboom *et al.*, 2012; Bo *et al.*, 2018), while a decrease in Drp1 activity is related to the phosphorylation at serine 637 (Knott, Perkins *et al.*, 2008a). The immunosuppressant drug **FK506**, a calcineurin inhibitor, commonly used to prevent organ rejection prevents dephosphorylation of serine 637 and has been shown to be therapeutically beneficial in ischaemic-perfusion injury with improved LV function and with TEM showing a preserved mitochondrial morphology (Sharp *et al.*, 2014). Significantly, by employing a phosphomimetic mutant corresponding to serine 637, the Frost study (Kalia *et al.,* 2018) additionally provided a structural basis for how phosphorylation at this site impairs Drp1 binding to MiD49. **Metformin** commonly used to treat type 2 diabetes, to lower blood sugar levels, has also been recently reported to preserve mitochondrial integrity through increased phosphorylation of Drp1 at serine 637 leading to the inhibition of Drp1 activity (Li *et al.,* 2016). Additional the cardioprotective effects of metformin have been linked to reduce atherosclerosis, induced by suppressing Drp1-mediated fission in endothelial cells (Wang *et al.,* 2017). Collectively, these studies support a strategy of inhibiting fission as a viable therapy in the setting of heart failure.

The studies highlighted above provide excellent examples of how cryo-EM and SPA can now generate high-resolution structures of mitochondrial proteins alone and in complex with adaptor molecules. The delineation of atomic resolution structures of protein–protein interaction sites represents an important step forward for developing new compounds to inhibit the interactions and regulate mitochondrial molecular pathways, and thus, cryo-EM is now poised to play a pivotal role in advancing these endeavours.

Electron tomography and mitochondrial membrane structure

Electron tomography (ET) is an application of TEM for the 3-D reconstruction of microstructural features within tissue slices or organelles (e.g. isolated mitochondria). Although

the gold standard for tissue preparation is fixation, embedding and staining to protect the specimen against beam damage, high vacuum and improve sample contrast, cryo-ET methods have also been developed to preserve specimens closer to their native environments; for a recent methodological review, see Pinali and Kitmitto (2014). The use of organic chemicals and embedding processes can, under some circumstances, lead to an osmotic imbalance, tissue damage and shrinkage, factors which spurred the development of freezing techniques. As with all techniques, there are limitations and practical considerations, but it should be noted that chemical fixation does not necessarily introduce artefacts, as illustrated by the morphological comparison of the cardiac dyad architecture [the spatial relationship between the sarcoplasmic reticulum (SR) and transverse tubules] showing no effect upon cellular morphology when compared to cryo-preserved samples (Hayashi *et al.,* 2009). As fixation and embedding methods are routine and relatively simple compared to cryo-techniques, it still often remains the first method of choice before advancing to cryogenic sample preparation methods.

Unlike cryo-EM of isolated proteins in order to capture different views/orientations of the tissue sections by ET, the sample is tilted around the stage axis taking an image at each tilt (typically in increments of 1–2°). The specimen is then rotated by 90° in the X-Y plane within the microscope to collect a second (dual) tilt series. ET is analogous to the technology used by computer axial tomography scanners with specialized image analysis software to generate 3-D reconstructions or tomograms by combining all the tilt images using back-projection algorithms. While the details that are resolved are not as high as cryo-EM and SPA, that is, typically 2–5 nm in the X-Y plane, membrane structures and macromolecular complexes are resolvable. The details in the Z-direction are limited by the thickness of the section. The introduction of FEGs as an electron source has also benefited ET methods, with a greater penetrative depth into the specimen facilitating the study of tissue sections up to 500 nm. For a recent detailed overview of cryo-ET, see Beck and Baumeister (2016).

ET for delineating respiratory complex organization in situ

While cryo-EM and SPA techniques can generate high-resolution structures for isolated proteins and complexes, an important development for advancing the understanding of their role in cellular processes and networks is the structural visualization within the native environment. This realization paved the way for developing approaches to integrate the single particle data (or X-ray crystallography or NMR structures) within the tomographic reconstructions, as recently reviewed by Baumeister and colleagues (Asano *et al.,* 2016). Accordingly, methods based upon subtomogram averaging, pattern recognition using template-matching algorithms, cross-correlation methods and statistical analysis techniques have been developed (Lucic *et al.,* 2005). An elegant example of the application of cryo-ET to investigate the spatial organization proteins and complexes within their native membrane environment is a study from Kuhlbrandt and colleagues mapping the organization of **ATPase synthase** (often referred to

as Complex V) and Complex I within the cristae (Davies *et al.,* 2014). By using a method of subtomogram averaging whereby sections of the tomogram are extracted and averaged to improve the signal : noise, they were able to show that ATP synthase form dimers that are distributed in rows along the curved regions of the inner leaflet of the cristae. In contrast, Complex I appeared to be randomly arranged on each side of the rows of ATPase synthase. The same group also recently identified that F-type ATPase dimers (at 2.6 nm resolution) in cilitate *Paramecium tetraurelia* form helical arrays that decorate tubular cristae; the functional significance of rows of the Complex has been suggested to be for optimization of ATP production (Muhleip *et al.,* 2016).

The application of ET for characterizing cristae architecture

ET methods were first employed over 20 years ago to reconstruct in 3-D mitochondria from rat and chick liver, revealing new details of the relationships between the IMM and OMM and the cristae organization (Perkins *et al.,* 1997) as well as the relationship with the endoplasmic reticulum (Mannella *et al.,* 1998). Significantly, 3-D data derived from ET methods have been pivotal for resolving the controversy surrounding cristae structure, which arose in part due to the limitations of 2-D TEM imaging of sections with mitochondria presenting different orientations within the tissue slices. Studies using conventional TEM demonstrated that the tips of the cristae folds often came close but did not fuse to the inner leaflet of the OMM (referred to as the inner boundary membrane, IBM). The organization of the cristae, the juxtaposition of the IMM with the IBM and volume of the matrix were subsequently related to the mitochondrial respiration state (Hackenbrock, 1966). However, it was only with the application of ET by Frey and colleagues that details of the cristae morphology and relationship with the IBM were uncovered in neuronal mitochondria from chick and rat. The tomograms revealed that the OMM and IMM were each ~7 nm thick and that IMM forms distinct junctions at the IBM, which are now termed cristae junctions, with diameters that are consistent in mitochondria from different species and tissue types and, further, that tubular cristae can merge to form 'lamellar compartments' (Perkins *et al.,* 1997). The 3-D datasets additionally allowed the measurement of the distance between the OMM and IMM. However, an important issue flagged by this study is that while chemical fixation of the tissue samples did not alter the distribution and dimensions of the cristae junctions, the distance between the OMM and IMM was reduced when compared to cryo-preserved samples (Frey and Mannella, 2000; Perkins and Frey, 2000), illustrating the point above regarding the importance of sample preparation methods. Frey and colleagues (Frey and Mannella, 2000; Perkins and Frey, 2000) also made the important observation that the number of cristae junctions was labile in response to cell stress. Further investigations then demonstrated that the cristae junctions range from 12 to 40 nm in diameter (Nicastro *et al.,* 2000; Perkins *et al.,* 2003) leading to the suggestion that they are intra-mitochondrial control points regulating protein, lipid and metabolite movement and, thus, are morphological mediators of OXPHOS (Mannella, 2006). These studies led to a new understanding of cristae morphology and revision of standard textbook images, based upon Palade's images from the 1950s.

Regulators of cristae morphology

ET studies of tissue from genetic models of protein ablation have been pivotal for establishing the link between cellular structure and function, an approach applied to investigate the role of fission and fusion proteins for mediating mitochondrial morphology and cristae structure. For example, using this approach, Scorrano and colleagues (Frezza *et al.,* 2006) showed that Opa1, a 120 kDa integral membrane protein, localized to the IMM protects against apoptosis by stabilizing the cristae morphology and integrity of the cristae junctions, which prevents the release of cytochrome c, building upon an earlier report by Olichon *et al.* (2003). Opa1 stabilizes the cristae junction through oligomerization of a membrane bound form, Opa-L and a soluble form Opa-S (Frezza *et al.,* 2006). Ablation of Opa1 is shown to result in disorganized cristae morphology, reduced mitochondrial membrane potential and OXPHOS activity (Cogliati *et al.,* 2013). The same study showed, importantly, that mitochondrial fragmentation could be rescued by Opa1-L but not Opa1-S. Similarly, ablation of Opa1 ($Opa1^{+/-}$) leading to a 50% reduction in expression in the heart has also been shown to result in increased cardiac mitochondrial heterogeneity, with an irregular organization of IFM with deformed and fragmented cristae (determined by standard TEM). The properties of the mitochondrial permeability transition pore were also altered in the knockout mice, with an associated Ca^{2+} leak. Furthermore, although there was no change to cardiac function due to partial Opa1 depletion alone, upon application of stress by transaortic constriction, leading to pressure overload, the mutant mice exhibited a doubling in hypertrophy with a reduced ejection fraction (43 vs. 22%) compared to the wild-type mice (Piquereau *et al.,* 2012). Consequently, these and other studies have inspired an interest in developing strategies to regulate Opa1 expression and function; for a comprehensive account of Opa1 as a therapeutic target in the heart, see Burke *et al.* (2015). Cleavage of Opa1-L to form Opa1-S with removal of the transmembrane anchor occurs under stress conditions in response to pro-apoptotic stimuli, loss of membrane potential and drop in ATP levels (Baricault *et al.,* 2007). The association between Opa1 cleavage and stabilization of cristae has led to approaches that block the formation of Opa1-S as a therapeutic strategy for preserving cristae integrity and function. Lee and colleagues (An *et al.,* 2013) demonstrated that deletion of hypoxia-induced gene domain protein-1a (Higd-1a) led to the formation of Opa1-S with mitochondrial disorganization and cristae disarray and so suggested that regulating expression of Higd-1a may have therapeutic benefits for preserving mitochondrial morphology. However, it is becoming clear that it is naïve to consider the short form as 'bad' and the long as 'good' as, while the long form can restore and promote mitochondrial fusion, a balance between the Opa1 isoforms has been shown to be necessary for maintenance of mitochondrial bioenergetic properties (Song *et al.,* 2007). Additionally in the setting of ischaemia–reperfusion damage, Opa1-S has been indicated as having a cardioprotective role (Sanjuan Szklarz and Scorrano, 2012). A further complication of targeting Opa1 is that activity is also regulated by post-translational

modification (Makino *et al.,* 2011). Makino and colleagues have shown that neonatal cardiomyocytes cultured in high concentrations of glucose (35 mM compared to normal media with 5 mM glucose) exhibit reduced expression of Opa1 and Mfn1, with the formation of *O*-GlcNAcylation of Opa1 and mitochondrial fragmentation. While the overexpression of Opa1 rescued the mitochondrial morphology reinforcing a causative link between mitochondrial dysmorphology and Opa1 expression, the study significantly showed that the post-translationally modified Opa1 contributes towards mitochondrial fragmentation. These data highlight the added complexes of drug development, and in this case targeting Opa1, in the clinical setting of diabetes. The picture is further complicated by recent studies identifying a multi-component complex termed mitochondrial contact site and cristae organizing system (MICOS) that mediates cristae biogenesis (Huynen *et al.,* 2016), with Opa1 binding to a component of MICOS (Glytsou *et al.,* 2016). A cartoon summarizing how alterations to Opa1-L may impact upon mitochondrial function is shown in Figure 1B. Additionally, Scorrano and colleagues demonstrated by cryo-ET that the organization of the respiratory Complexes underpinning OXPHOS is dependent upon the cristae structure, with cristae remodelling identified as a feature of heart failure (Cogliati *et al.,* 2016). In summary, although the last 30 years have seen major advances towards understanding cristae morphology, there are still critical gaps in the knowledge surrounding the factors that drive cristae formation and control microstructural features.

The role of ET for delineating inter-mitochondrial communication

Elegant studies by Hajnóczky and colleagues (Eisner *et al.,* 2017) have recently imaged mitochondrial fusion events within the whole rat heart illustrating content mixing between two fusing mitochondria. Adenoviral transfection of mitochondrial matrix-targeted proteins with engineered fluorescent tags importantly led to the identification of two types of fusion events, with rapid (<12 s) and slow (>12 s) kinetics. Rapid fusion was attributed to the amalgamation of two juxtaposed mitochondrion (as depicted in Figure 1A), whereas slow fusion events were proposed to occur between two non-adjacent mitochondria *via* mitochondrial nanotunnels. Mitochondrial nanotunnels are evolutionarily-conserved structures identified in prokaryotic and eukaryotic cell types but have only been fairly recently identified in the heart by both TEM and confocal microscopy showing mitochondria extensions proposed to facilitate communications with non-adjacent mitochondrion separated by up to 8 μm (Huang *et al.,* 2013); an exemplar TEM image of a cardiac mitochondrial nanotunnel is presented in Figure 2A. Given the physical constraints of particularly the IFM in cardiac tissue by myofibrils, the concept of nanotunnels extending over many microns to facilitate communication between non-adjacent mitochondria has generated a lot of interest and focus for research especially in the context of disease conditions (Vincent *et al.,* 2016). However, what is not yet clear is whether mitochondrial nanotunnels are a result of impaired fission or represent a compensatory-adaptive process. Additionally, in

the heart, it is not established whether the nanotunnel tip forms a type of junction with the connecting mitochondrion (Figure 2B), which transfers a signal to the partnering mitochondria, and/or if the signal mediated at the junction will always eventually trigger fusion joining the two mitochondria. The diameter of the tunnels, measuring between 90 and 210 nm (Huang *et al.,* 2013), would feasibly facilitate the transport and mixing of small molecules such as mtDNA, proteins and metabolites upon fusion; for a detailed overview see Vincent *et al.* (2017).

ET has recently been employed to further develop the current understanding of nanotunnel structures for propagating inter-mitochondrial communication over relatively long distances within the cardiomyocyte by Lavorato *et al.* (2017). The group showed that the nanotunnel frequency was increased in the myocardium of a transgenic mouse with a mutation in the calcium release channel, **ryanodine receptor**, $RyR2^{A4860G+/-}$, compared to wild-type mice. The RyR2 mutation identified in patients with catecholaminergic polymorphic ventricular tachycardia results in a loss of channel function with sporadic Ca^{2+} bursts during systole due to SR overload leading to elevated Ca^{2+} levels promoting arrhythmogenesis. Standard TEM and ET were employed to investigate nanotunnel architecture and showed that they are composed of both the OMM and IMM with the cristae extending through the protrusion, proposed to facilitate inter-mitochondrial matrix content transfer. Further analysis of the tomograms revealed that many small mitochondria were actually cross sections through tunnels, highlighting how reports of small fragmented mitochondria by standard 2-D imaging may actually represent portions through nanotunnels and not a result of increased fission and the importance of 3-D imaging techniques. Additionally, the 3-D reconstructions of the mitochondria revealed that the cristae are aligned to the tunnel long-axis consistent with proposals that microtubules through a 'pulling action' are involved in nanotunnel elongation (Wang *et al.,* 2015); in contrast, in the skeletal muscle, the nanotunnels were described as being devoid of cristae (Vincent *et al.,* 2017). Moreover, the identification of increased nanotunneling activity, but slower kinetics of inter-mitochondrial mixing in the heterozygous mouse $RyR2^{A4860G+/-}$ model also indicates that Ca^{2+} homeostasis may play a role in nanotunnel formation, with slow rates of communication due to increased distances over which content-exchange occurs. Although a caveat to this interpretation is the effect of the mutation itself upon matrix-exchange, which could not be excluded. These data also raised the interesting possibility of whether the process of content transfer drives nanotunnel extension or if the tunnels must form first.

Specialized structures between adjacent cardiac mitochondria, termed inter-mitochondrial junctions (IMJs), were first characterized in the 1980s using TEM methods and described as regions between the OMM of two abutting mitochondria that are 'electron-dense zones', with contact surfaces ranging from ~0.1 to 0.9 microns in diameter (Bakeeva *et al.,* 1982). Similar structures were subsequently identified in the frog heart (Duvert *et al.,* 1985). Using ET methods, IMJs have been further characterized, advancing the understanding of the pivotal role these structures play in establishing long-range mitochondrial communication
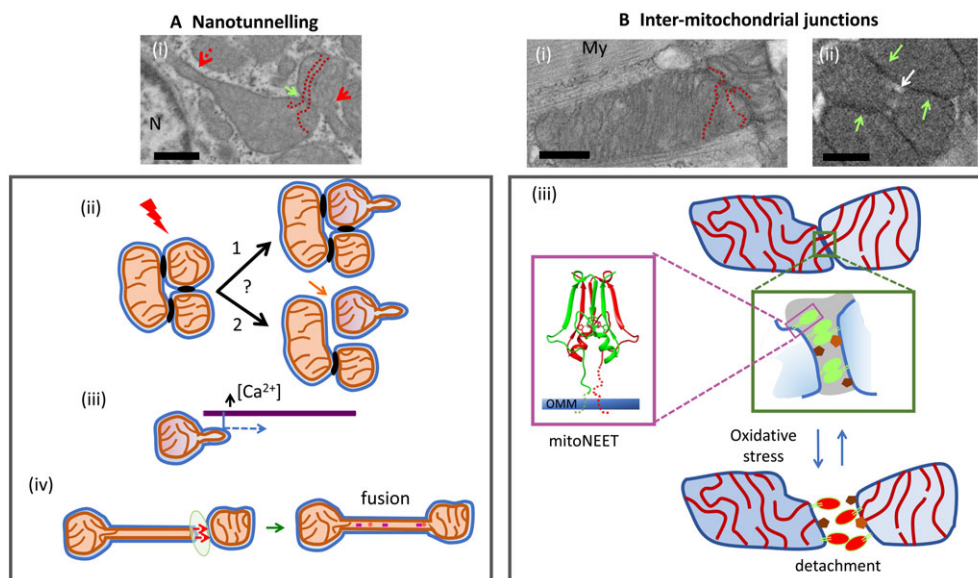
Figure 2

Communication between adjacent and non-adjacent mitochondria for maintaining network quality control. (A) Electron micrograph (TEM) shows a protrusion, a putative 'nanotunnel' from a perinuclear mitochondrion (left-ventricle) that extends nearly 1 micron (dashed red arrow). Another nanotunnel (solid red arrow) can be seen to form a physical contact with another mitochondrion. Within the same figure, IMJs (green arrow) can be resolved with alignment of cristae (dashed orange lines delineate the cristae). N, nucleus. Scale bar = 500 nm. (ii–iv) Cartoon depicting the putative formation of mitochondrial nanotunnels. (ii) A stimulus (physiological or pathological, indicated by the red lightning bolt) is proposed to promote nanotube formation. It is not clear if a nanotube forms on a mitochondrion while still connected to the energy network (route 1); IMJs depicted in black, or if the nanotube starts to form in response to a mitochondrion being detached from the grid, indicated by the orange arrow (route 2). The micrograph in (i) would support route 1 but is only one example and may also not represent the mechanism in disease conditions. (iii) Microtubules (purple rod) are involved in nanotube extension to form tunnels (Vincent *et al.*, 2017) with Ca^{2+} homeostasis also proposed to play a central role (Lavorato *et al.*, 2017). (iv) Two putative forms of nanotunnel communication are shown, where the tubular extension formed by the OMM and IMM (cartoon based upon Vincent *et al.*, 2017) forms contacts but do not merge with another mitochondrion (dashed red arrows indicate transfer of information and shaded area the nanotunnel junction) and secondly where the nanotunnel fuses with the partnering mitochondrion. The molecular content within the nanotunnel junctional space is not known nor is whether the signalling pathways always promote fusion to allow the transfer and mixing of small molecules such as proteins, mitochondrial DNA (represented by the squares and circles). (B, i) An exemplar TEM shows two adjacent cardiac (murine left ventricle) mitochondria flanked on either side by myofibrils (My). Scale bar = 500 nm. The figure illustrates how the cristae from the two mitochondria are aligned and appear almost continuous between the two mitochondrion (cristae morphology mapped with dashed orange lines). The region where the two mitochondrion are touching is the IMJ. (ii) Exemplar region of a serial SBF-SEM image (left ventricle) showing how at lower resolution the spaces between the neighbouring mitochondria are observed as electron dense regions (indicated by the green arrows). Interestingly, in the example shown, there appear to be two projections linking two mitochondria; the identity of these densities is unknown. Scale bars = 500 nm. (iii) A cartoon illustrating how at the IMJ the cristae are aligned with the lower image showing a putative junctional area in more detail. While all of the molecular components within the IMJ have yet to be identified (depicted by the brown blocks), the protein mNT (depicted by the green shape) has been suggested to be a key component regulating IMJ morphology by acting as a tether to link two adjacent mitochondrion. The crystal structure of mNT has been determined as shown in the purple box (pdb: 2QD0), corresponding to amino acids 33–108. The dashed lines represent the missing amino-terminal target sequence and membrane anchoring transmembrane helix. It has been demonstrated by several groups that the IMJs are labile and act to not only tether mitochondria together but also function as 'safety valves' to isolate dysfunctional mitochondria from the cell-wide network (Glancy *et al.*, 2017), but the mechanisms involved have yet to be delineated. The cartoon speculates that the redox activity of the mNT [2Fe-S] clusters could potentially be involved as a molecular switch in response to oxidative stress to change the conformation of mNT (now shown as red/green shape) and hence tethering properties; this concept is based upon the study from Landry *et al.* (2015). Understanding the dynamics of IMJ morphology, mechanisms of plasticity and the molecular identity of the proteins within the junctions is now the next challenge, especially since the molecules and process of tethering and disengagement represent potential therapeutic targets.

networks (Picard *et al.*, 2015). Picard and colleagues used tomograms to reconstruct the regions formed between mitochondria, IMJs, and revealed that there is a structural co-ordination and alignment between cristae from adjacent mitochondria, as illustrated in Figure 2B. Work from Paukov and Protsenko (1996) had previously showed, using standard TEM, that IMJs are labile, increasing and decreasing in number in response to cardiomyocyte activity associated with cardiac pathologies, including hypertrophy and ischaemia,

leading to the suggestion that a change to IMJ density is an early adaptive remodelling event to compensate for increased load. By investigating IMJ morphology in different tissue types, Picard *et al.* (2015) subsequently reported that IMJ density can be correlated to the energy requirements of the cell type and accordingly are most abundant between cardiac mitochondria. Based upon the defined structural architecture and links to metabolic demands, IMJs are suggested to be central for signal propagation between nearby

mitochondria. IMJs are now established as a key component of the mitochondrial structural architecture, underpinning the formation of an energy supply network in the heart (Glancy *et al.,* 2017).

In summary, the above studies illustrate the pivotal contribution that ET methods have made towards the current body of knowledge of mitochondrial morphology and development of cell-wide communication networks. Moreover, what is clear from these studies is the power of ET methods for probing nanoscale morphological details of mitochondria with future potential application for investigating key outstanding questions surrounding how IMJ properties and nanotunnel contacts, fusion and frequency, are remodelled as heart failure develops and their contribution to the progression of mitochondrial dysfunction. As these important questions and others are addressed, structure–function-based research will undoubtedly greatly benefit from ET methods towards the hunt for new therapeutic strategies for, for example, stabilizing cristae architecture and maintaining the quality and energy distribution networks essential for cardiac function. Additionally, compared to cryo-EM and SPA, the impact of DEDs upon the resolution of tomograms has yet to be fully realized, but combined with image analysis techniques such as sub-tomographic averaging and technological advancements including the Volta phase plate, the details emerging from tomographic 3-D reconstructions are now likely to be achieved at much higher resolutions (Khoshouei *et al.*, 2017a).

Volume scanning electron microscopy for investigating mitochondrial structure and function

As previously discussed, in the heart mitochondria typically span the length of a sarcomere ~2 μm; therefore, depending upon the orientation of the mitochondria within a tissue slice <500 nm thick, an incomplete and possibly misleading view of the organelle may appear in 2-D micrographs from standard TEM. Furthermore, as discussed earlier, mitochondrial nanotunnels extending over several microns can move out of the plane of the thin section. Therefore, while the magnification employed will dictate the field of view in the X-Y plane, the Z-direction is linked to the section thickness. Recently, a modification of an SEM to examine blocks of tissue up to 0.5 mm^3 was developed, SBF-SEM (Denk and Horstmann, 2004). Additionally, another configuration of SEM using a focussed ion beam (FIB)-SEM also became available commercially (Knott *et al.,* 2008b). Analysing blocks of tissue allows cellular structures to be examined in relation to the surrounding structural architecture, adding another layer of biological information. In both instruments, the surface of the specimen is removed either by a microtome positioned within the microscope, which slices off a section 50–100 nm thick (SBF-SEM) or by ion milling 20–50 nm (FIB-SEM); in each case, it is the newly exposed block face that is imaged. The removal of a slice from the tissue is an iterative procedure, so that a stack of images is generated through the sample forming a 3-D dataset. Both of these methods of 'volumetric microscopy' have pros and cons, as reviewed by

Pinali and Kitmitto (2014). The main difference between the two techniques is that the field of view is smaller for FIB-SEM compared to SBF-SEM, but the attainable resolution in the Z-direction is higher. For SBF-SEM, we routinely collect data at between 10 and 12 nm per pixel in the X-Y plane and 50 nm in the Z-direction (Pinali *et al.,* 2017). However, the rate-limiting step for both SBF-SEM and FIB-SEM is the data analysis. While there are ongoing endeavours to develop automated software to extract details of cellular properties (e.g. Hussain *et al.,* 2018), currently, structures within the 3-D dataset are generally analysed by manual segmentation using ET software such as IMOD (Kremer *et al.,* 1996), as exemplified in Figure 3. As mentioned earlier, we reported that in an ovine tachypacing-induced model of end-stage heart failure, the mitochondria were severely disorganized; these investigations employed SBF-SEM of tissue sampled from the left ventricle (Pinali *et al.,* 2013). As the 3-D datasets contain structural details at the whole cardiomyocyte level, we were also able to investigate the spatial relationship between the mitochondria and SR by segmenting both features, revealing a loss of inter-organelle communication, which will lead to impaired Ca^{2+} uptake from the SR into the mitochondria and, therefore, likely be a contributing factor for the development of mitochondrial dysfunction. Furthermore, as well as providing qualitative data, we were able to quantify the mitochondrial density showing an increase in the failing myocardium compared to control. Whether the increase in mitochondrial number is a result of stalled mitophagy, with the accumulation of damaged mitochondria, or an adaptive response to generate more mitochondria in efforts to meet the bioenergetics demands of tachypacing and, subsequently, a failing myocardium is unknown. The study by Glancy *et al.* (2017) establishing the role of IMJs and mitochondrial connectivity in both heart and skeletal muscle employed FIB-SEM with the 3-D reconstructions of mitochondrial populations within different regions of the cell providing a structural framework to explain mitochondrial electrical coupling and the role of 'sub-networks'. Significantly, the study also demonstrated how the plasticity of IMJ connectivity also serves as a safety mechanism for rapid disengagement and isolation of impaired mitochondria from the system. Nanotubes were also observed within the PNM group, but were infrequent, forming in less than 10% of the mitochondria.

An exciting new development of FIB-SEM is cryo-FIB-SEM whereby frozen hydrated samples can be analysed without the need for chemical fixation (Schertel *et al.,* 2013; Rigort and Plitzko, 2015). Schertel *et al.* applied this technique to frozen murine optic nerve specimens and demonstrated that the contrast was sufficient to allow 3-D reconstruction of the mitochondria and cristae. Furthermore, different physical features of the mitochondria in the oligodendrocyte and astrocytic process were resolvable (with voxel size in the X, Y, Z directions of 7.5:7.5:30 nm).

The application of volumetric microscopy for investigating IMJ organization

There is still limited knowledge surrounding the molecular identity of the proteins within, and forming the IMJ, or how these proteins and the IMJ architecture are remodelled
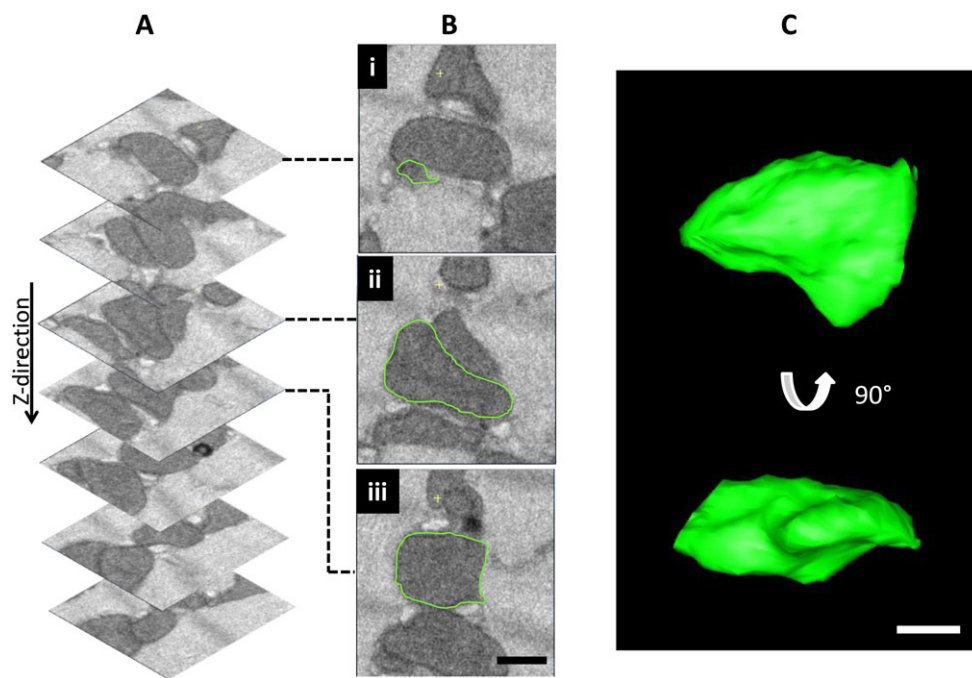
Figure 3

3-D reconstruction of a murine cardiac mitochondrion using SBF-SEM reveals an elongated irregular shape. (A) Exemplar serial images (50 nm cut-depth in Z-direction) collected by SBF-SEM of tissue taken from the murine LV [data collected for a voxel size 13.3:13.3:50 nm (X:Y:Z)]. For clarity, only every other image at a 100 nm interval is displayed. (B, i) A mitochondrion, outlined (segmented) in green, when it first becomes visible in the stack; (ii) 300 nm deeper into the image stack and the mitochondrion now appears to have a tubular shape. (iii) After another 100 nm [400 nm from image (i)], the same mitochondrion appears almost square shaped. (C) Segmentation of the highlighted mitochondrion using IMOD (Kremer *et al.,* 1996) through the image stack reveals the 3-D structure as viewed from two different orientations. By segmenting the mitochondrion, physical parameters such as volume and surface area can be calculated: for example, the mitochondrion displayed has a volume of 6.55×10^{8} nm^3 and surface area of 4.20×10^{6} nm^2. Scale bars = 500 nm. These data show how the position and orientation of a mitochondrion within a thin section may give a different impression of the morphology dependent upon where it is located. The figure also illustrates how SBF-SEM can be used to quantify the physical parameters of individual mitochondria and so has an application as a diagnostic tool for investigating morphological changes to mitochondria under pathological and experimental conditions.

in response to cardiovascular complications such as heart failure. Cosson and colleagues identified the protein mitoNEET, mNT, as important for IMJ formation (Colca *et al.,* 2004). It has since been shown that mNT forms dimers, with the suggestion that mNT from each neighbouring mitochondria interact to form a tether between mitochondria for IMJ formation (Vernay *et al.,* 2017). Crystallization of mNT showed that it forms a dimer with c2 symmetry (Conlan *et al.,* 2009). The cytoplasmic domains referred to as 'tethering arms' were determined to be highly flexible leading to two conformations: whether dimers of dimers form *in vivo* and if this is regulated by the 'tethering arms' adopting a specific orientation to form an inter-mitochondrial link is currently not clear. Interestingly, in a heart tissue extract, the mNT [2Fe-S] clusters were shown to undergo redox transition in response to H_2O_2 (Landry *et al.,* 2015); the authors therefore proposed that oxidative stress may be a regulator of mNT function. Interestingly, the same study showed that oxidation is reversible and the clusters could revert back to the reduced state (the predominant state *in vivo*); it is, therefore, intriguing to speculate if the redox state of the [2Fe-S] clusters could lead to protein conformational changes sufficient to impact upon the morphology of the IMJs and thus be a factor regulating energy transmission (as summarized in the lower panel of Figure 2B). Vernay *et al*. (2017) also showed, by using FIB-SEM, coupled with 2-D TEM, to investigate mitochondrial morphology in mNT knockout mouse embryonic fibroblast cells, that while the size of mitochondria did not change, the number of IMJs was reduced. Knock-in studies further confirmed the role of mNT in IMJ formation, showing increased mitochondrial clustering with an increased number of IMJs; significantly, in cells expressing high levels of mNT there was excessive clustering of the mitochondria, which also led to disruption of the mitochondrial network. Furthermore, the formation of IMJs was shown to be independent of fusion events facilitated by Mfn1 and Mfn2. Cardiac mitochondria from a mouse model of global mNT ablation were shown to have reduced oxidative capacity compared to those isolated from wild-type mice, indicating that mNT plays an important role in mitochondrial function in the heart (Wiley *et al.,* 2007). The same study also showed that mNT is mostly highly expressed in the heart compared to the liver, adipose tissue and skeletal muscle.

While a detailed understanding of mNT function remains to be determined, there are now several studies showing a direct link to not only IMJ formation but also mitochondrial bioenergetics and mitophagy (Lazarou *et al.,* 2013). Consequently, there is much interest in the potential of mNT as a

drug target for treating mitochondrial dysfunction; for a detailed review, see Geldenhuys *et al.* (2014). Colca and colleagues (Colca *et al.,* 2004) also showed that mNT binds **pioglitazone**, the hyperglycaemic drug used for treating diabetes. Pioglitazone–mNT binding has been demonstrated to stabilize mNT, and it is this interaction that has been proposed to be one of the factors underpinning the beneficial effects of pioglitazone observed clinically (Paddock *et al.,* 2007). Several derivatives of pioglitazone have since been synthesized, MSDC-0160 and MSDC-0602, which bind to mNT (Bolten *et al.,* 2007). *In vivo* experiments with control mice and diabetic KKAy mice treated with MSDC-0160 were shown to have increased expression of mNT and improved insulin-sensitization. Since then, MSDC-0160 has been the subject of clinical trials in patients with type 2 diabetes and also Alzheimer patients (Shah *et al.,* 2014). Although it is not currently known how IMJs are remodelled in heart failure, mNT over-expression in the atrial cell line HL-1 has been indicated to have a cardioprotective role against oxidative cell stress (Habener *et al.,* 2016).

Conclusions and future perspectives

This review has highlighted several examples of the fundamental contributions that EM techniques have made towards understanding mitochondrial function and, importantly, dysfunction in human disease, with a focus upon heart failure. The emerging developments in EM hardware, software, methods for data integration and multi-scale analyses have catapulted 3-D EM techniques into a new era of structural biology; as summarized in Figure 4. In particular, cryo-EM and SPA methods for determining near atomic resolution protein structures have moved this technique from being considered a niche specialist research area to one with potential for investment within the drug industry, especially since data collection and processing are becoming more streamlined and automated. With the application of cryo-EM to previously elusive membrane protein structures, often the gatekeepers of signalling pathways, we are likely to see an exponential increase in the discovery and design of structure-based ligands for therapeutic purposes. In addition to enabling drug design,
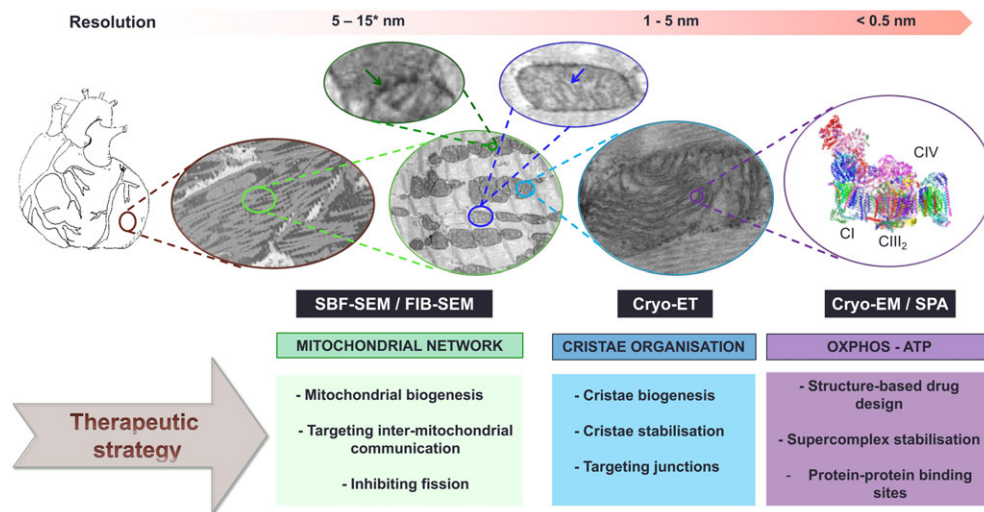
Figure 4

Illustration of how 3-D EM techniques straddle the biological structural hierarchy and how each of these methods can contribute towards therapeutic strategies and drug development. Tissue taken from the heart can be biopsied for SBF-SEM and FIB-SEM sampling up to ~0.5 mm^3. Using either of these 3-D SEM modalities, cardiomyocytes can be analysed *in situ*, with the data sets revealing cardiomyocyte size, shape, organization and structural relationships with other cell types, for example, fibroblasts and the extracellular matrix. Data sets collected at higher magnification can reveal details of the cellular structure of cardiomyocytes, for example, the image with the brown border is a portion taken from an SBF-SEM data stack (murine left ventricle) with a voxel size of ~13.3 nm in the X:Y plane and 50 nm in the Z-direction. From these data, mitochondrial network formation and spatial distribution can be analysed. Higher magnifications can be employed as demonstrated by the serial image with a light green border, taken from an SBF-SEM dataset collected at a voxel size of 6.8:6.8:50 nm (X:Y:Z); the magnified areas shown above illustrate how densities between mitochondria (image with dark green border, with putative connections indicated by the arrow) and outline of the cristae (image with dark blue border) can also be visualized (indicated by the dark blue arrow). TEM methods, cryo-ET, can be employed in a complementary approach to investigate details of the OMM, IMM and cristae morphology and large macromolecular complexes of tissue slices up to 500 nm thick; the exemplar image (light blue border) shows an interfibrillar mitochondrion within a tissue section from the left ventricle illustrating the tubular cristae organization. Moving up the resolution scale, cryo-TEM has seen a huge advancement in capabilities for the study of single proteins and complexes using SPA methods to generate 3-D structures now at near to atomic resolution. The structure surrounded by the purple border shows the respirasome [downloaded from the RCSB Protein Data Bank, 5J4Z, (Letts *et al.,* 2016) and modelled using UCSF Chimera (Pettersen *et al.,* 2004)]. This structure illustrates how the cutting-edge developments of cryo-EM and SPA methods now have the capabilities to aid structure-based drug design to enter a new era of discovery. For each of the 3-D EM techniques, we have summarized in colour-coded boxes the applications of each of these modalities to advance therapeutic discoveries targeting the key areas of mitochondrial function and dysfunction as discussed in this review. The approximate resolution of structural data obtainable from each of these EM techniques is illustrated along the top of the image (* indicates the nm/pixel in the X:Y plane only).

high-resolution structures for the individual respiratory Complexes and the respirasome will now aid clinical understanding of how genetic mutations in, for example, metabolic conditions (Pereira *et al.,* 2011) translate through to modifications in protein and membrane structure and bioenergetic dysfunction (as reviewed by Lloyd and McGeehan, 2013).

The integration of structural data from each of the 3-D EM modalities also shows promise with advances in algorithms and modelling software already facilitating the fitting of high-resolution structures from SPA methods into lower resolution EM envelopes from ET. There still remain several issues that need to be overcome for multi-scale data integration; notwithstanding the computational challenges, there are also problems surrounding how to determine the molecular identity of the protein and complex components *in situ* within the tomogram. However, as evidenced by the recent hardware and software advances, these goals are more than realistic and the ability to generate tomograms at higher resolution and improved contrast will be additionally instrumental for achieving structural data integration. A further development will be the incorporation of tomograms within SBF-SM and FIB-SEM data sets, or *vice-versa*, that is, where the analysis of larger specimens by volumetric methods are used to target the location of specific cellular features within a tissue sample; the same block (this is straightforward for plastic blocks) can then be removed and sectioned for TEM to collect a tomographic data set at higher resolutions. While outside the scope of this review, it is also worth noting that there is currently much interest in cross-scale structural analysis, interfacing of live cell imaging with EM techniques, with a particular interest in its assimilation with FIB-SEM and SBF-SEM methods (Fermie *et al.,* 2018). Combining live cell imaging methods with EM methods (CLEM) will allow dynamic cellular processes (and effects and mechanisms of pharmacological agents) to be correlated with nanostructural changes. While there are technical challenges around developing integrated imaging pipelines, including sample preparation methods, tracking of molecular entities that can be visualized by both imaging modalities, matching regions of interest, the outlook is very promising and is poised to provide yet another quantum leap for drug discovery.

In conclusion, bioenergetic abnormalities are a feature of a wide range of human diseases, including heat failure, and targeting energy imbalances presents as an attractive therapeutic approach. EM studies and biochemical analyses, as highlighted earlier, suggest that there are three distinct mitochondrial populations in the cardiomyocyte, and as such, targeting cardiac mitochondria may have an added layer of complexity as each different population may be affected differently by the same therapeutic compound. Whether the structure–function variations are indeed linked to spatial locations or a result of mainly imaging in 2-D with biochemical differences arising as a result of isolation methods is still not fully clear. However, the application of SBF-SEM and FIB-SEM to study mitochondria networks in whole cells *in situ* will be central for advancing investigations to resolve questions surrounding mitochondrial distribution and communication. In conclusion, heart failure leads to a poor quality of life; it is ultimately a terminal illness complicated by co-morbidities and as such places an enormous economic burden upon our healthcare system. New heart failure treatments are therefore of high priority; the recent advances in 3-D EM techniques are now positioning these methods to make a central contribution for expediting and advancing drug discovery in this area.

Nomenclature of targets and ligands

Key protein targets and ligands in this article are hyperlinked to corresponding entries in http://www.guidetopharmacology.org, the common portal for data from the IUPHAR/BPS Guide to PHARMACOLOGY (Harding *et al.,* 2018), and are permanently archived in the Concise Guide to PHARMACOLOGY 2017/18 (Alexander *et al.,* 2017a,b,c,d).

Acknowledgements

Conflict of interest

The authors declare no conflicts of interest.

References

Acin-Perez R, Fernandez-Silva P, Peleato ML, Perez-Martos A, Enriquez JA (2008). Respiratory active mitochondrial supercomplexes. Mol Cell 32: 529–539.

Afsar B, Ortiz A, Covic A, Solak Y, Goldsmith D, Kanbay M (2016). Focus on renal congestion in heart failure. Clin Kidney J 9: 39–47.

Alexander SPH, Christopoulos A, Davenport AP, Kelly E, Marrion NV, Peters JA *et al.* (2017a). The Concise Guide to PHARMACOLOGY 2017/18: G protein-coupled receptors. Br J Pharmacol 174: S17–S129.

Alexander SPH, Fabbro D, Kelly E, Marrion NV, Peters JA, Faccenda E *et al.* (2017b). The Concise Guide to PHARMACOLOGY 2017/18: Enzymes. Br J Pharmacol 174: S272–S359.

Alexander SPH, Kelly E, Marrion NV, Peters JA, Faccenda E, Harding SD *et al.* (2017c). The Concise Guide to PHARMACOLOGY 2017/18: Transporters. Br J Pharmacol 174: S360–S446.

Alexander SP, Striessnig J, Kelly E, Marrion NV, Peters JA, Faccenda E *et al.* (2017d). The Concise Guide to PHARMACOLOGY 2017/18: voltage-gated ion channels. Br J Pharmacol 174: S160–S194.

An HJ, Cho G, Lee JO, Paik SG, Kim YS, Lee H (2013). Higd-1a interacts with Opa1 and is required for the morphological and functional integrity of mitochondria. Proc Natl Acad Sci U S A 110: 13014–13019.

Archer SL (2013). Mitochondrial dynamics – mitochondrial fission and fusion in human diseases. New Engl J Med 369: 2236–2251.

Asano S, Engel BD, Baumeister W (2016). In situ cryo-electron tomography: a post-reductionist approach to structural biology. J Mol Biol 428: 332–343.

Ayesta A, Martinez-Selles H, Bayes de Luna A, Martinez-Selles M (2018). Prediction of sudden death in elderly patients with heart failure. J Geriatr Cardiol 15: 185–192.

Bakeeva LE, Chentsov I, Skulachev VP (1982). Intermitochondrial contacts of cardiomyocytes. Tsitologiia 24: 161–166.

Baricault L, Segui B, Guegand L, Olichon A, Valette A, Larminat F et al. (2007). OPA1 cleavage depends on decreased mitochondrial ATP level and bivalent metals. Exp Cell Res 313: 3800–3808.

Basu K, Lajoie D, Aumentado-Armstrong T, Chen J, Koning RI, Bossy B et al. (2017). Molecular mechanism of DRP1 assembly studied in vitro by cryo-electron microscopy. PLoS One 12: e0179397.

Beck M, Baumeister W (2016). Cryo-electron tomography: can it reveal the molecular sociology of cells in atomic detail? Trends Cell Biol 26: 825–837.

Bo T, Yamamori T, Suzuki M, Sakai Y, Yamamoto K, Inanami O (2018). Calmodulin-dependent protein kinase II (CaMKII) mediates radiation-induced mitochondrial fission by regulating the phosphorylation of dynamin-related protein 1 (Drp1) at serine 616. Biochem Biophys Res Commun 495: 1601–1607.

Bolten CW, Blanner PM, McDonald WG, Staten NR, Mazzarella RA, Arhancet GB et al. (2007). Insulin sensitizing pharmacology of thiazolidinediones correlates with mitochondrial gene expression rather than activation of PPAR gamma. Gene Regul Syst Bio 1: 73–82.

Bordt EA, Clerc P, Roelofs BA, Saladino AJ, Tretter L, Adam-Vizi V et al. (2017). The putative Drp1 inhibitor mdivi-1 is a reversible mitochondrial complex I inhibitor that modulates reactive oxygen species. Dev Cell 40: 583–594.e6.

Brown DA, Perry JB, Allen ME, Sabbah HN, Stauffer BL, Shaikh SR et al. (2017). Expert consensus document: mitochondrial function as a therapeutic target in heart failure. Nat Rev Cardiol 14: 238–250.

Bugger H, Abel ED (2010). Mitochondria in the diabetic heart. Cardiovasc Res 88: 229–240.

Burke N, Hall AR, Hausenloy DJ (2015). OPA1 in cardiovascular health and disease. Curr Drug Targets 16: 912–920.

Camacho P, Fan H, Liu Z, He JQ (2016). Small mammalian animal models of heart disease. Am J Cardiovasc Dis 6: 70–80.

Cassidy-Stone A, Chipuk JE, Ingerman E, Song C, Yoo C, Kuwana T et al. (2008). Chemical inhibition of the mitochondrial division dynamin reveals its role in Bax/Bak-dependent mitochondrial outer membrane permeabilization. Dev Cell 14: 193–204.

Chaban Y, Boekema EJ, Dudkina NV (2014). Structures of mitochondrial oxidative phosphorylation supercomplexes and mechanisms for their stabilisation. Biochim Biophys Acta 1837: 418–426.

Chen Y, Liu Y, Dorn GW 2nd (2011). Mitochondrial fusion is essential for organelle function and cardiac homeostasis. Circ Res 109: 1327–1331.

Cheng Y, Grigorieff N, Penczek PA, Walz T (2015). A primer to single-particle cryo-electron microscopy. Cell 161: 438–449.

Cherubini M, Gines S (2017). Mitochondrial fragmentation in neuronal degeneration: toward an understanding of HD striatal susceptibility. Biochem Biophys Res Commun 483: 1063–1068.

Claude A, Fullam EF (1945). An electron microscope study of isolated mitochondria: method and preliminary results. J Exp Med 81: 51–62.

Cleland JG, Torabi A, Khan NK (2005). Epidemiology and management of heart failure and left ventricular systolic dysfunction in the aftermath of a myocardial infarction. Heart 91 (Suppl. 2): ii7–ii13; discussion ii31, ii43–18.

Cogliati S, Frezza C, Soriano ME, Varanita T, Quintana-Cabrera R, Corrado M et al. (2013). Mitochondrial cristae shape determines respiratory chain supercomplexes assembly and respiratory efficiency. Cell 155: 160–171.

Cogliati S, Enriquez JA, Scorrano L (2016). Mitochondrial cristae: where beauty meets functionality. Trends Biochem Sci 41: 261–273.

Colca JR, McDonald WG, Waldon DJ, Leone JW, Lull JM, Bannow CA et al. (2004). Identification of a novel mitochondrial protein ('mitoNEET') cross-linked specifically by a thiazolidinedione photoprobe. Am J Physiol Endocrinol Metab 286: E252–E260.

Conlan AR, Paddock ML, Axelrod HL, Cohen AE, Abresch EC, Wiley S et al. (2009). The novel 2Fe-2S outer mitochondrial protein mitoNEET displays conformational flexibility in its N-terminal cytoplasmic tethering domain. Acta Crystallogr Sect F Struct Biol Cryst Commun 65: 654–659.

Crochemore C, Mekki M, Corbière C, Karoui A, Noël R, Vendeville C et al. (2015). Subsarcolemmal and interfibrillar mitochondria display distinct superoxide production profiles. Free Radic Res 49 (3): 331–337.

Danev R, Baumeister W (2016). Cryo-EM single particle analysis with the Volta phase plate. Elife 5.

D'Aurelio M, Gajewski CD, Lenaz G, Manfredi G (2006). Respiratory chain supercomplexes set the threshold for respiration defects in human mtDNA mutant cybrids. Hum Mol Genet 15: 2157–2169.

Davies KM, Daum B, Gold VA, Muhleip AW, Brandt T, Blum TB et al. (2014). Visualization of ATP synthase dimers in mitochondria by electron cryo-tomography. J Vis Exp. https://doi.org/ 10.3791/51228.

Denk W, Horstmann H (2004). Serial block-face scanning electron microscopy to reconstruct three-dimensional tissue nanostructure. PLoS Biol 2: e329.

Dietl A, Maack C (2017). Targeting mitochondrial calcium handling and reactive oxygen species in heart failure. Curr Heart Fail Rep 14: 338–349.

Disatnik MH, Ferreira JC, Campos JC, Gomes KS, Dourado PM, Qi X et al. (2013). Acute inhibition of excessive mitochondrial fission after myocardial infarction prevents long-term cardiac dysfunction. J Am Heart Assoc 2: e000461.

Dorn GW 2nd (2013a). Mitochondrial dynamics in heart disease. Biochim Biophys Acta 1833: 233–241.

Dorn GW 2nd (2013b). Mitochondrial dynamism and cardiac fate – a personal perspective. Circ J 77: 1370–1379.

Dubochet J, Adrian M, Chang J-J, Homo J-C, Lepault J, McDowall AW et al. (1988). Cryo-electron microscopy of vitrified specimens. Q Rev Biophys 21: 129–228.

Duvert M, Mazat JP, Barets AL (1985). Intermitochondrial junctions in the heart of the frog, Rana esculenta. A thin-section and freeze-fracture study. Cell Tissue Res 241: 129–137.

Eisner V, Cupo RR, Gao E, Csordas G, Slovinsky WS, Paillard M et al. (2017). Mitochondrial fusion dynamics is robust in the heart and depends on calcium oscillations and contractile activity. Proc Natl Acad Sci U S A 114: E859–E868.

Facundo H, Brainard RE, Caldas FRL, Lucas AMB (2017). Mitochondria and cardiac hypertrophy. Adv Exp Med Biol 982: 203–226.

Fala L (2015). Entresto (Sacubitril/Valsartan): First-in-class angiotensin receptor neprilysin inhibitor FDA approved for patients with heart failure. Am Health Drug Benefits 8: 330–334.

Fermie J, Liv N, Ten Brink C, van Donselaar EG, Muller WH, Schieber NL et al. (2018). Single organelle dynamics linked to 3D structure by correlative live-cell imaging and 3D electron microscopy. Traffic 19: 354–369.

Fernandez-Leiro R, Scheres SHW (2017). A pipeline approach to single-particle processing in RELION. Acta Crystallogr D Struct Biol 73: 496–502.

Filichia E, Hoffer B, Qi X, Luo Y (2016). Inhibition of Drp1 mitochondrial translocation provides neural protection in dopaminergic system in a Parkinson's disease model induced by MPTP. Sci Rep 6: 32656.

Frey TG, Mannella CA (2000). The internal structure of mitochondria. Trends Biochem Sci 25: 319–324.

Frezza C, Cipolat S, Martins de Brito O, Micaroni M, Beznoussenko GV, Rudka T et al. (2006). OPA1 controls apoptotic cristae remodeling independently from mitochondrial fusion. Cell 126: 177–189.

Frohlich C, Grabiger S, Schwefel D, Faelber K, Rosenbaum E, Mears J et al. (2013). Structural insights into oligomerization and mitochondrial remodelling of dynamin 1-like protein. EMBO J 32: 1280–1292.

Galloway CA, Yoon Y (2015). Mitochondrial dynamics in diabetic cardiomyopathy. Antioxid Redox Signal 22: 1545–1562.

Geldenhuys WJ, Leeper TC, Carroll RT (2014). mitoNEET as a novel drug target for mitochondrial dysfunction. Drug Discov Today 19: 1601–1606.

Givvimani S, Munjal C, Tyagi N, Sen U, Metreveli N, Tyagi SC (2012). Mitochondrial division/mitophagy inhibitor (Mdivi) ameliorates pressure overload induced heart failure. PLoS One 7: e32388.

Glancy B, Hartnell LM, Combs CA, Femnou A, Sun J, Murphy E et al. (2017). Power grid protection of the muscle mitochondrial reticulum. Cell Rep 19: 487–496.

Glytsou C, Calvo E, Cogliati S, Mehrotra A, Anastasia I, Rigoni G et al. (2016). Optic atrophy 1 is epistatic to the core MICOS component MIC60 in mitochondrial cristae shape control. Cell Rep 17: 3024–3034.

Gomez LA, Monette JS, Chavez JD, Maier CS, Hagen TM (2009). Supercomplexes of the mitochondrial electron transport chain decline in the aging rat heart. Arch Biochem Biophys 490: 30–35.

Gonzalez A, Ravassa S, Beaumont J, Lopez B, Diez J (2011). New targets to treat the structural remodeling of the myocardium. J Am Coll Cardiol 58: 1833–1843.

Gu J, Wu M, Guo R, Yan K, Lei J, Gao N et al. (2016). The architecture of the mammalian respirasome. Nature 537: 639–643.

Guo R, Zong S, Wu M, Gu J, Yang M (2017). Architecture of human mitochondrial respiratory megacomplex I2III2IV2. Cell 170: 1247–1257 e1212.

Habener A, Chowdhury A, Echtermeyer F, Lichtinghagen R, Theilmeier G, Herzog C (2016). MitoNEET protects HL-1 cardiomyocytes from oxidative stress mediated apoptosis in an in vitro model of hypoxia and reoxygenation. PLoS One 11: e0156054.

Hackenbrock CR (1966). Ultrastructural bases for metabolically linked mechanical activity in mitochondria. I. Reversible ultrastructural changes with change in metabolic steady state in isolated liver mitochondria. J Cell Biol 30: 269–297.

Harding SD, Sharman JL, Faccenda E, Southan C, Pawson AJ, Ireland S et al. (2018). The IUPHAR/BPS Guide to PHARMACOLOGY in 2018: updates and expansion to encompass the new guide to IMMUNOPHARMACOLOGY. Nucl Acids Res 46: D1091–D1106.

Hatano A, Okada J, Washio T, Hisada T, Sugiura S (2015). Distinct functional roles of cardiac mitochondrial subpopulations revealed by a 3D simulation model. Biophys J 108: 2732–2739.

Hayashi T, Martone ME, Yu Z, Thor A, Doi M, Holst MJ et al. (2009). Three-dimensional electron microscopy reveals new details of membrane systems for Ca2+ signaling in the heart. J Cell Sci 122: 1005–1013.

Henderson R (2015). Overview and future of single particle electron cryomicroscopy. Arch Biochem Biophys 581: 19–24.

Hendgen-Cotta UB, Esfeld S, Jastrow H, Totzeck M, Altschmied J, Goy C et al. (2018). Mouse cardiac mitochondria do not separate in subsarcolemmal and interfibrillar subpopulations. Mitochondrion 38: 1–5.

Hollander JM, Thapa D, Shepherd DL (2014). Physiological and structural differences in spatially distinct subpopulations of cardiac mitochondria: influence of cardiac pathologies. Am J Physiol Heart Circ Physiol 307: H1–H14.

Huang X, Sun L, Ji S, Zhao T, Zhang W, Xu J et al. (2013). Kissing and nanotunneling mediate intermitochondrial communication in the heart. Proc Natl Acad Sci U S A 110: 2846–2851.

Hussain A, Ghosh S, Kalkhoran SB, Hausenloy DJ, Hanssen E, Rajagopal V (2018). An automated workflow for segmenting single adult cardiac cells from large-volume serial block-face scanning electron microscopy data. J Struct Biol 202: 275–285.

Huynen MA, Muhlmeister M, Gotthardt K, Guerrero-Castillo S, Brandt U (2016). Evolution and structural organization of the mitochondrial contact site (MICOS) complex and the mitochondrial intermembrane space bridging (MIB) complex. Biochim Biophys Acta 1863: 91–101.

Kalia R, Wang RY, Yusuf A, Thomas PV, Agard DA, Shaw JM et al. (2018). Structural basis of mitochondrial receptor binding and constriction by DRP1. Nature 558: 401–405.

Khan SS, Butler J, Gheorghiade M (2014). Management of comorbid diabetes mellitus and worsening heart failure. JAMA 311: 2379–2380.

Khoshouei M, Pfeffer S, Baumeister W, Forster F, Danev R (2017a). Subtomogram analysis using the Volta phase plate. J Struct Biol 197: 94–101.

Khoshouei M, Radjainia M, Baumeister W, Danev R (2017b). Cryo-EM structure of haemoglobin at 3.2 A determined with the Volta phase plate. Nat Commun 8: 16099.

Knott AB, Perkins G, Schwarzenbacher R, Bossy-Wetzel E (2008a). Mitochondrial fragmentation in neurodegeneration. Nat Rev Neurosci 9: 505–518.

Knott G, Marchman H, Wall D, Lich B (2008b). Serial section scanning electron microscopy of adult brain tissue using focused ion beam milling. J Neurosci 28: 2959–2964.

Knowlton AA, Liu TT (2015). Mitochondrial dynamics and heart failure. Compr Physiol 6: 507–526.

Kremer JR, Mastronarde DN, McIntosh JR (1996). Computer visualization of three-dimensional image data using IMOD. J Struct Biol 116: 71–76.

Kubli DA, Gustafsson AB (2012). Mitochondria and mitophagy; the yin and yang of cell death control. Circ Res 111: 1208–1221.

Kuhlbrandt W (2014). Biochemistry. The resolution revolution. Science 343: 1443–1444.

Landry AP, Cheng Z, Ding H (2015). Reduction of mitochondrial protein mitoNEET [2Fe-2S] clusters by human glutathione reductase. Free Radic Biol Med 81: 119–127.

Lavorato M, Iyer VR, Dewight W, Cupo RR, Debattisti V, Gomez L et al. (2017). Increased mitochondrial nanotunneling activity, induced by calcium imbalance, affects intermitochondrial matrix exchanges. Proc Natl Acad Sci U S A 114: E849–E858.

Lazarou M, Narendra DP, Jin SM, Tekle E, Banerjee S, Youle RJ (2013). PINK1 drives Parkin self-association and HECT-like E3 activity upstream of mitochondrial binding. J Cell Biol 200: 163–172.

Letts JA, Fiedorczuk K, Sazanov LA (2016). The architecture of respiratory supercomplexes. Nature 537: 644–648.

Li A, Zhang S, Li J, Liu K, Huang F, Liu B (2016). Metformin and resveratrol inhibit Drp1-mediated mitochondrial fission and prevent ER stress-associated NLRP3 inflammasome activation in the adipose tissue of diabetic mice. Mol Cell Endocrinol 434: 36–47.

Lloyd RE, McGeehan JE (2013). Structural analysis of mitochondrial mutations reveals a role for bigenomic protein interactions in human disease. PLoS One 8: e69003.

Lobo-Jarne T, Ugalde C (2018). Respiratory chain supercomplexes: structures, function and biogenesis. Semin Cell Dev Biol 76: 179–190.

Lucic V, Forster F, Baumeister W (2005). Structural studies by electron tomography: from cells to molecules. Annu Rev Biochem 74: 833–865.

Luu M, Stevenson WG, Stevenson LW, Baron K, Walden J (1989). Diverse mechanisms of unexpected cardiac arrest in advanced heart failure. Circulation 80: 1675–1680.

Makino A, Suarez J, Gawlowski T, Han W, Wang H, Scott BT et al. (2011). Regulation of mitochondrial morphology and function by O-GlcNAcylation in neonatal cardiac myocytes. Am J Physiol Regul Integr Comp Physiol 300: R1296–R1302.

Mannella CA (2006). Structure and dynamics of the mitochondrial inner membrane cristae. Biochim Biophys Acta 1763: 542–548.

Mannella CA, Buttle K, Rath BK, Marko M (1998). Electron microscopic tomography of rat-liver mitochondria and their interaction with the endoplasmic reticulum. Biofactors 8: 225–228.

Maranzana E, Barbero G, Falasca AI, Lenaz G, Genova ML (2013). Mitochondrial respiratory supercomplex association limits production of reactive oxygen species from complex I. Antioxid Redox Signal 19: 1469–1480.

Marsboom G, Toth PT, Ryan JJ, Hong Z, Wu X, Fang YH et al. (2012). Dynamin-related protein 1-mediated mitochondrial mitotic fission permits hyperproliferation of vascular smooth muscle cells and offers a novel therapeutic target in pulmonary hypertension. Circ Res 110: 1484–1497.

McCarron JG, Wilson C, Sandison ME, Olson ML, Girkin JM, Saunter C et al. (2013). From structure to function: mitochondrial morphology, motion and shaping in vascular smooth muscle. J Vasc Res 50: 357–371.

McMullan G, Faruqi AR, Henderson R (2016). Direct electron detectors. Methods Enzymol 579: 1–17.

Milani-Nejad N, Janssen PM (2014). Small and large animal models in cardiac contraction research: advantages and disadvantages. Pharmacol Ther 141: 235–249.

Minicucci MF, Azevedo PS, Polegato BF, Paiva SA, Zornoff LA (2011). Heart failure after myocardial infarction: clinical implications and treatment. Clin Cardiol 34: 410–414.

Moreno-Lastres D, Fontanesi F, Garcia-Consuegra I, Martin MA, Arenas J, Barrientos A et al. (2012). Mitochondrial complex I plays an essential role in human respirasome assembly. Cell Metab 15: 324–335.

Muhleip AW, Joos F, Wigge C, Frangakis AS, Kuhlbrandt W, Davies KM (2016). Helical arrays of U-shaped ATP synthase dimers form tubular cristae in ciliate mitochondria. Proc Natl Acad Sci U S A 113: 8442–8447.

Nicastro D, Frangakis AS, Typke D, Baumeister W (2000). Cryo-electron tomography of neurospora mitochondria. J Struct Biol 129: 48–56.

Okoshi MP, Capalbo RV, Romeiro FG, Okoshi K (2017). Cardiac cachexia: perspectives for prevention and treatment. Arq Bras Cardiol 108: 74–80.

Olichon A, Baricault L, Gas N, Guillou E, Valette A, Belenguer P et al. (2003). Loss of OPA1 perturbates the mitochondrial inner membrane structure and integrity, leading to cytochrome c release and apoptosis. J Biol Chem 278: 7743–7746.

Oliphant CS, Owens RE, Bolorunduro OB, Jha SK (2016). Ivabradine: a review of labeled and off-label uses. Am J Cardiovasc Drugs 16: 337–347.

Ong SB, Subrayan S, Lim SY, Yellon DM, Davidson SM, Hausenloy DJ (2010). Inhibiting mitochondrial fission protects the heart against ischemia/reperfusion injury. Circulation 121: 2012–2022.

Osellame LD, Singh AP, Stroud DA, Palmer CS, Stojanovski D, Ramachandran R et al. (2016). Cooperative and independent roles of the Drp1 adaptors Mff, MiD49 and MiD51 in mitochondrial fission. J Cell Sci 129: 2170–2181.

Otera H, Wang C, Cleland MM, Setoguchi K, Yokota S, Youle RJ et al. (2010). Mff is an essential factor for mitochondrial recruitment of Drp1 during mitochondrial fission in mammalian cells. J Cell Biol 191: 1141–1158.

Paddock ML, Wiley SE, Axelrod HL, Cohen AE, Roy M, Abresch EC et al. (2007). MitoNEET is a uniquely folded 2Fe 2S outer mitochondrial membrane protein stabilized by pioglitazone. Proc Natl Acad Sci U S A 104: 14342–14347.

Palade GE (1952). The fine structure of mitochondria. Anat Rec 114: 427–451.

Paukov VS, Protsenko DD (1996). The intermitochondrial contacts of cardiomyocytes during cardiac adaptation under pathological conditions. Arkh Patol 58: 43–50.

Pereira L, Soares P, Radivojac P, Li B, Samuels DC (2011). Comparing phylogeny and the predicted pathogenicity of protein variations reveals equal purifying selection across the global human mtDNA diversity. Am J Hum Genet 88: 433–439.

Perkins GA, Frey TG (2000). Recent structural insight into mitochondria gained by microscopy. Micron 31: 97–111.

Perkins G, Renken C, Martone ME, Young SJ, Ellisman M, Frey T (1997). Electron tomography of neuronal mitochondria: three-dimensional structure and organization of cristae and membrane contacts. J Struct Biol 119: 260–272.

Perkins GA, Ellisman MH, Fox DA (2003). Three-dimensional analysis of mouse rod and cone mitochondrial cristae architecture: bioenergetic and functional implications. Mol Vis 9: 60–73.

Pettersen EF, Goddard TD, Huang CC, Couch GS, Greenblatt DM, Meng EC *et al.* (2004). UCSF Chimera – a visualization system for exploratory research and analysis. J Comput Chem 25: 1605–1612.

Picard M, McManus MJ, Csordas G, Varnai P, Dorn GW 2nd, Williams D *et al.* (2015). Trans-mitochondrial coordination of cristae at regulated membrane junctions. Nat Commun 6: 6259.

Pinali C, Kitmitto A (2014). Serial block face scanning electron microscopy for the study of cardiac muscle ultrastructure at nanoscale resolutions. J Mol Cell Cardiol 76: 1–11.

Pinali C, Bennett H, Davenport JB, Trafford AW, Kitmitto A (2013). Three-dimensional reconstruction of cardiac sarcoplasmic reticulum reveals a continuous network linking transverse-tubules: this organization is perturbed in heart failure. Circ Res 113: 1219–1230.

Pinali C, Malik N, Davenport JB, Allan LJ, Murfitt L, Iqbal MM *et al.* (2017). Post-myocardial infarction t-tubules form enlarged branched structures with dysregulation of junctophilin-2 and bridging integrator 1 (BIN-1). J Am Heart Assoc 6: pii: e004834.

Piquereau J, Caffin F, Novotova M, Prola A, Garnier A, Mateo P *et al.* (2012). Down-regulation of OPA1 alters mouse mitochondrial morphology, PTP function, and cardiac adaptation to pressure overload. Cardiovasc Res 94: 408–417.

Ponikowski P, Anker SD, AlHabib KF, Cowie MR, Force TL, Hu S *et al.* (2014). Heart failure: preventing disease and death worldwide. ESC Heart Fail 1: 4–25.

Qi X, Qvit N, Su YC, Mochly-Rosen D (2013). A novel Drp1 inhibitor diminishes aberrant mitochondrial fission and neurotoxicity. J Cell Sci 126: 789–802.

Rigort A, Plitzko JM (2015). Cryo-focused-ion-beam applications in structural biology. Arch Biochem Biophys 581: 122–130.

Rimbaud S, Garnier A, Ventura-Clapier R (2009). Mitochondrial biogenesis in cardiac pathophysiology. Pharmacol Reps: PR 61: 131–138.

Riva A, Tandler B, Loffredo F, Vazquez E, Hoppel C (2005). Structural differences in two biochemically defined populations of cardiac mitochondria. Am J Physiol Heart Circ Physiol 289: H868–H872.

Rosca MG, Vazquez EJ, Kerner J, Parland W, Chandler MP, Stanley W *et al.* (2008). Cardiac mitochondria in heart failure: decrease in respirasomes and oxidative phosphorylation. Cardiovasc Res 80: 30–39.

Sanjuan Szklarz LK, Scorrano L (2012). The antiapoptotic OPA1/Parl couple participates in mitochondrial adaptation to heat shock. Biochim Biophys Acta 1817: 1886–1893.

Schagger H, Pfeiffer K (2000). Supercomplexes in the respiratory chains of yeast and mammalian mitochondria. EMBO J 19: 1777–1783.

Schertel A, Snaidero N, Han HM, Ruhwedel T, Laue M, Grabenbauer M *et al.* (2013). Cryo FIB-SEM: volume imaging of cellular ultrastructure in native frozen specimens. J Struct Biol 184: 355–360.

Scheubel RJ, Tostlebe M, Simm A, Rohrbach S, Prondzinsky R, Gellerich FN *et al.* (2002). Dysfunction of mitochondrial respiratory chain complex I in human failing myocardium is not due to disturbed mitochondrial gene expression. J Am Coll Cardiol 40: 2174–2181.

Schwarzer M, Schrepper A, Amorim PA, Osterholt M, Doenst T (2013). Pressure overload differentially affects respiratory capacity in interfibrillar and subsarcolemmal mitochondria. Am J Physiol Heart Circ Physiol 304: H529–H537.

Shah RC, Matthews DC, Andrews RD, Capuano AW, Fleischman DA, VanderLugt JT *et al.* (2014). An evaluation of MSDC-0160, a prototype mTOT modulating insulin sensitizer, in patients with mild Alzheimer's disease. Curr Alzheimer Res 11: 564–573.

Sharp WW, Fang YH, Han M, Zhang HJ, Hong Z, Banathy A *et al.* (2014). Dynamin-related protein 1 (Drp1)-mediated diastolic dysfunction in myocardial ischemia-reperfusion injury: therapeutic benefits of Drp1 inhibition to reduce mitochondrial fission. FASEB J 28: 316–326.

Sharp WW, Beiser DG, Fang YH, Han M, Piao L, Varughese J *et al.* (2015). Inhibition of the mitochondrial fission protein dynamin-related protein 1 improves survival in a murine cardiac arrest model. Crit Care Med 43: e38–e47.

Sharpley MS, Shannon RJ, Draghi F, Hirst J (2006). Interactions between phospholipids and NADH:ubiquinone oxidoreductase (complex I) from bovine mitochondria. Biochemistry 45: 241–248.

Shimada T, Horita K, Murakami M, Ogura R (1984). Morphological studies of different mitochondrial populations in monkey myocardial cells. Cell Tissue Res 238: 577–582.

Sjostrand FS (1956). The ultrastructure of cells as revealed by the electron microscope. Int Rev Cytol 5: 455–533.

Smith G, Gallo G (2017). To mdivi-1 or not to mdivi-1: is that the question? Dev Neurobiol 77: 1260–1268.

Song Z, Chen H, Fiket M, Alexander C, Chan DC (2007). OPA1 processing controls mitochondrial fusion and is regulated by mRNA splicing, membrane potential, and Yme1L. J Cell Biol 178: 749–755.

Sousa JS, Mills DJ, Vonck J, Kuhlbrandt W (2016). Functional asymmetry and electron flow in the bovine respirasome. Elife 5.

Strait JB, Lakatta EG (2012). Aging-associated cardiovascular changes and their relationship to heart failure. Heart Fail Clin 8: 143–164.

Taguchi N, Ishihara N, Jofuku A, Oka T, Mihara K (2007). Mitotic phosphorylation of dynamin-related GTPase Drp1 participates in mitochondrial fission. J Biol Chem 282: 11521–11529.

Taylor CJ, Ryan R, Nichols L, Gale N, Hobbs FR, Marshall T (2017). Survival following a diagnosis of heart failure in primary care. Fam Pract 34: 161–168.

Thompson RF, Walker M, Siebert CA, Muench SP, Ranson NA (2016). An introduction to sample preparation and imaging by cryo-electron microscopy for structural biology. Methods 100: 3–15.

Vernay A, Marchetti A, Sabra A, Jauslin TN, Rosselin M, Scherer PE *et al.* (2017). MitoNEET-dependent formation of intermitochondrial junctions. Proc Natl Acad Sci U S A 114: 8277–8282.

Vincent AE, Ng YS, White K, Davey T, Mannella C, Falkous G *et al.* (2016). The spectrum of mitochondrial ultrastructural defects in mitochondrial myopathy. Sci Rep 6: 30610.

Vincent AE, Turnbull DM, Eisner V, Hajnoczky G, Picard M (2017). Mitochondrial Nanotunnels. Trends Cell Biol 27: 787–799.

Wang C, Du W, Su QP, Zhu M, Feng P, Li Y *et al.* (2015). Dynamic tubulation of mitochondria drives mitochondrial network formation. Cell Res 25: 1108–1120.

Wang Q, Zhang M, Torres G, Wu S, Ouyang C, Xie Z *et al.* (2017). Metformin suppresses diabetes-accelerated atherosclerosis via the inhibition of Drp1-mediated mitochondrial fission. Diabetes 66: 193–205.

Wiley SE, Murphy AN, Ross SA, van der Geer P, Dixon JE (2007). MitoNEET is an iron-containing outer mitochondrial membrane protein that regulates oxidative capacity. Proc Natl Acad Sci U S A 104: 5318–5323.

Winge DR (2012). Sealing the mitochondrial respirasome. Mol Cell Biol 32: 2647–2652.

Wolters FJ, Segufa RA, Darweesh SKL, Bos D, Ikram MA, Sabayan B *et al*. (2018). Coronary heart disease, heart failure, and the risk of dementia: a systematic review and meta-analysis. Alzheimers Dement pii: S1552-5260(18)30026-8.

Zheng SQ, Palovcak E, Armache JP, Verba KA, Cheng Y, Agard DA (2017). MotionCor2: anisotropic correction of beam-induced motion for improved cryo-electron microscopy. Nat Methods 14: 331–332.

Zhu J, Vinothkumar KR, Hirst J (2016). Structure of mammalian respiratory complex I. Nature 536: 354–358.